Icarus **152**, 384–406 (2001)
doi:10.1006/icar.2001.6632, available online at http://www.idealibrary.com on IDEAL®

Seasonal Variations of Titan's Atmospheric Composition

Sébastien Lebonnois

Centre d'Etude Spatiale des Rayonnements, 9 av. du Col. Roche, B.P. 4346, F-31028 Toulouse Cedex 04, France, and NASA Ames Research Center, MS 245-3, Moffett Field, California 94035-1000
E-mail: lebonnois@cesr.fr

Dominique Toublanc

Centre d'Etude Spatiale des Rayonnements, 9 av. du Col. Roche, B.P. 4346, F-31028 Toulouse Cedex 04, France

Frederic Hourdin

Laboratoire de Météorologie Dynamique, Jussieu, CNRS/UPMC, Box 99, F-75252 Paris Cedex 05, France

and

Pascal Rannou

Service d'Aéronomie, Jussieu, CNRS/UPMC, F-75252 Paris Cedex 05, France

Received March 13, 2000; revised February 26, 2001; Posted online June 27, 2001

In order to investigate seasonal variations of the composition of Titan's low stratosphere, we developed a two-dimensional (latitude–altitude) photochemical and transport model. Large-scale advection, hidden in the vertical eddy diffusion for one-dimensional models, is accounted for explicitly. Atmospheric dynamics is prescribed using results of independent numerical simulations of the atmospheric general circulation. Both the mean meridional transport and latitudinal mixing by transient planetary waves are taken into account. Chemistry is based on 284 reactions involving 40 hydrocarbons and nitriles. Photodissociation rates are based on a three-dimensional description of the ultraviolet flux. For most species, the model fits well the latitudinal variations observed by Voyager I giving for the first time a full and self-consistent interpretation of these observations. In particular, the enrichment of the high northern latitudes is attributed to subsidence during the winter preceeding the Voyager encounter. Discrepancies are observed for C_2H_4, HC_3N, and C_2N_2 and are attributed to problems in the chemical scheme. Sensitivity to dynamical parameters is investigated. The vertical eddy diffusion coefficient keeps an important role for the upper atmosphere. The wind strength and horizontal eddy diffusion strongly control the latitudinal behavior of the composition in the low stratosphere, while mean concentrations appear to be essentially controlled by chemistry.

Key Words: **Titan; photochemistry; atmospheres—composition; atmospheres—dynamics.**

1. INTRODUCTION

To understand the complex photochemistry in the atmosphere of Titan, several photochemical models have been developed, computing the composition as a function of altitude, under equatorial or disk-averaged conditions; see Strobel (1982), Yung *et al*. (1984), Yung (1987), Toublanc *et al*. (1995), and Lara *et al*. (1996). In these one-dimensional models, dynamical processes are parameterized as a vertical eddy diffusion. The mixing coefficient is fitted as a function of altitude in order to reproduce the observations, and especially the HCN vertical profile retrieved from ground-based millimeter and submillimeter observations (Tanguy *et al*. 1990 and Hidayat *et al*. 1997). One-dimensional models concentrated on the interpretation of planetary averaged or equatorial observations. The latitudinal contrasts in the composition of the low stratosphere observed by Voyager I at spring equinox (Coustenis and Bézard 1995) have not been extensively investigated. In particular, the enrichment in the high northern latitudes in most species is not yet understood. In a previous study (Lebonnois and Toublanc 1999), we developed a three-dimensional description of the ultraviolet flux to test the latitudinal sensitivity of composition profiles obtained with a one-dimensional photochemical model. This study showed that radiation and chemistry alone could not explain the observations. An important missing piece in these studies is the large-scale atmospheric dynamics. Chemical concentrations generally

0019-1035/01 $35.00

increase as a function of altitude between the surface and the source region at several hundred kilometers. It is thus expected that downward (upward) winds should increase (decrease) local concentrations.

In this paper, we investigate this effect with a latitude–altitude photochemical and transport model. The photochemistry is heritated from Toublanc *et al.* (1995) and presented in Section 2.2. Computation of photodissociation rates uses the full 3-D description of the UV flux mentioned above. The main advance in this paper is to introduce the two-dimensional transport of chemical species. Mean meridional transport is computed with a finite volume transport scheme (Van Leer 1977, Hourdin and Armengaud 1999) using meridional and vertical winds matching the general circulation model (GCM) results (Hourdin *et al.* 1995) as explained in Section 2.3. The effect of transient eddies is also accounted for based on a horizontal diffusion operator. The main results are presented in Section 3. The latitudinal contrasts compare generally well with Voyager observations, with an enrichment in nitriles and hydrocarbons by a factor of 2 to 10. In the simulation, this enrichment is unambiguously attributed to the effect of subsidence in the northern high latitudes during the winter season which preceeds the Voyager encounter, bringing chemical species down from the source region. Section 4 presents systematic sensitivity studies of the model to eddy diffusion coefficients (vertical and horizontal), strength of the winds, and the phase of the seasonal changes in the circulation.

2. DESCRIPTION OF THE MODEL

The photochemical model includes 40 chemical compounds involved in 284 reactions (including photodissociations). These compounds are hydrocarbons and nitriles; oxygeneous compounds have not been included yet. All compounds with more than five heavy atoms (C,N) are treated as solid organic material and named "soot." This "soot" is a sink for photochemistry, and may be related to the source of Titan's haze. The latitude–altitude plane is divided into 17×130 cells, 10° wide in latitude and 10 km high (which gives four layers by scale height in the stratosphere). In this model, the troposphere is not well described (only two layers by scale height), but our main focus is on the low stratospheric composition as a function of time and latitude.

Temperature is prescribed as a function of altitude following Lellouch *et al.* (1989) below 250 km and Yelle (1991) above. This profile is kept fixed in latitude and time. Hourdin *et al.* (1995) explored with a GCM the structure of the lower part of the atmosphere (up to the stratopause, $\sim$250 km) and the temperature latitudinal variations have also been retrieved from VoyagerI/IRIS spectra for 0.4-mbar and 1-mbar levels (Flasar and Conrath 1990, Coustenis and Bézard 1995). In both cases, the variations have a maximum amplitude of $\sim$15 K. These variations have only a small effect on the chemical reaction rates and have therefore been neglected. It must also be kept in mind that there are important uncertainties in that many of the reaction rates have not been measured at the relevant temperatures for Titan's atmosphere. These uncertainties can have strong implications on the composition, as shown by recent studies on Neptune (Dobrijevic and Parisot 1998) and Titan (Smith 1999).

TABLE I
Mean Boundary Fluxes, in $cm^{-2} \cdot s^{-1}$
(Referred to the Surface)

Jeans escape for H	1.7×10^9
Jeans escape for H_2	7.3×10^9
N atoms[a]	2.5×10^8
Net destruction of CH_4	6.5×10^9

[a] Computed with the ionospheric model described in Galand *et al.* (1999).

The two seasonal major forcings in the model are the UV field and the meridional wind field in the 0–500 km range. The model also includes molecular diffusion, as well as vertical and horizontal eddy diffusion. The boundary fluxes are treated in the same way as in Toublanc *et al.* (1995): Jeans escape for H and H_2, dissociation of N_2 by magnetospheric electrons for N atoms, and CH_4 input flux at the surface, to balance the net destruction of methane. These fluxes are indicated in Table I. For other species, upper and lower boundaries are zero flux. Concerning the dissociation of N_2 by magnetospheric electrons, the downward flux of N atoms represents a source that is mainly located above 1000 km. The approximation we use (global source at 1300 km instead of a vertical distribution) has no significant influence in the lower atmosphere (below 600 km), on which we focus in this paper. The condensation of compounds around the tropopause is treated in a simple way: Any constituent is bound to remain under its saturation vapor pressure during the resolution of the continuity equation. Lara *et al.* (1996) used a more sophisticated treatment in their photochemical model, and concluded that no compounds (excluding CH_4) seemed to be supersaturated, justifying the use of simple treatments for condensation. Supersaturation is still possible for CH_4 in our model, and we used a supersaturation factor of 1.2 to get a mole fraction of 2% above the tropopause. The continuity equation is solved for each species as described by Toublanc *et al.* (1995), with the additional terms resulting from horizontal diffusion and dynamical transport by winds.

2.1. UV Field

A three-dimensional Monte-Carlo model has been used to get a complete description of the UV field, and diurnal means were computed as functions of time (15 different solar declinations) and of latitude. This model is described in detail in Lebonnois and Toublanc (1999). New absorption cross sections for C_4H_2 have been taken from Smith *et al.* (1998). Other cross sections are referenced in Table II. Dominant sources of opacity are indicated in Table III. The haze opacity and scattering properties

TABLE II
References Used for the Photoabsorption Cross Sections

Species	References
CH_3	Parkes *et al.* (1973)
CH_4	Hudson (1971), Mount *et al.* (1977), Samson *et al.* (1989)
C_2H_2	Cooper *et al.* (1995a), Smith *et al.* (1991)
C_2H_4	Cooper *et al.* (1995b), Zelikoff and Watanabe (1953)
C_2H_6	Okabe and Becker (1963), Mount and Moos (1978)
CH_3C_2H	Natayama and Watanabe (1964), Fahr and Nayak (1996)
CH_2CCH_2	Rabalais *et al.* (1971), Fuke and Schnepp (1979)
C_3H_6	Samson *et al.* (1962), Fahr and Nayak (1996)
C_3H_8	Okabe and Becker (1963), Calvert and Pitts (1966)
C_4H_2	Okabe (1981), Fahr and Nayak (1994), Smith *et al.* (1998)
C_4H_4	Fahr and Nayak (1996)
C_4H_6	Fahr and Nayak (1994)
N_2	Fennelly and Torr (1992)
HCN	Lee (1980), Nuth and Glicker (1982)
HC_3N	Connors *et al.* (1974), Bénilan *et al.* (1994)
C_2N_2	Connors *et al.* (1974), Bénilan (1998, private communication)

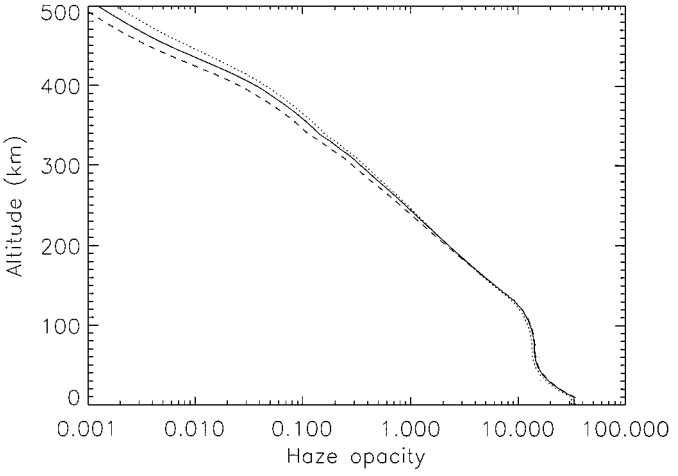

FIG. 1. Vertical profile of the haze opacity at 200 nm (dotted line), 250 nm (solid line), and 300 nm (dashed line).

of aerosols have been calculated with fractal particles (Rannou *et al.* 1995, Rannou *et al.* 1999). The vertical profile of the haze opacity is presented in Fig. 1. We do not include possible latitudinal and seasonal variations of this opacity at this stage.

Simultaneous computations of the UV radiative transfer and 2-D photochemistry would be too expensive. Instead, we use a sequential approach. Ultraviolet fluxes are first computed with a first guess of the concentration of chemical compounds (resulting from one-dimensional calculations). Those precomputed radiative constants are then used to run the two-dimensional photochemical model on a typical period of several Titan years. The equatorial composition as function of height is then used to make a new computation of the UV field. The photodissociation rates calculated for several species for spring equatorial conditions are displayed in Fig. 2, and two-dimensional maps (altitude–latitude) of the photodissociation coefficients of acetylene are presented in Fig. 3 for northern winter solstice and spring equinox. These variations are fairly representative of all the other species' photodissociation coefficients. At this stage, latitudinal variations of the chemical composition are not included in the UV computations. This adds an uncertainty on the diurnal means of the UV field, especially for high latitudes, but the dominant seasonal variations of the photodissociation rates are obtained with the three-dimensional calculations. Local variations of the opacity would affect essentially the region of absorption of a given wavelength. Our computations have confirmed that photodissociation rates and composition are not very sensitive to small variations of the gaseous and haze opacity.

TABLE III
Dominant Sources of UV Opacity

Component	Wavelength range	Absorption region
N_2	$\leq$100 nm	1000–1200 km
Methane	100–145 nm	600–800 km
Other gaseous species	145–200 nm	200–800 km
Aerosols	$\geq$180 nm	100–400 km

2.2. Chemistry

The photodissociation scheme used for CH_4 is the second scheme from Mordaunt *et al.* (1993):

$$CH_4 + h\nu \xrightarrow{0.49} CH_3 + H$$
$$CH_4 + h\nu \xrightarrow{0.51} CH + H_2 + H.$$

We have also tested the new scheme proposed by Smith and Raulin (1999)

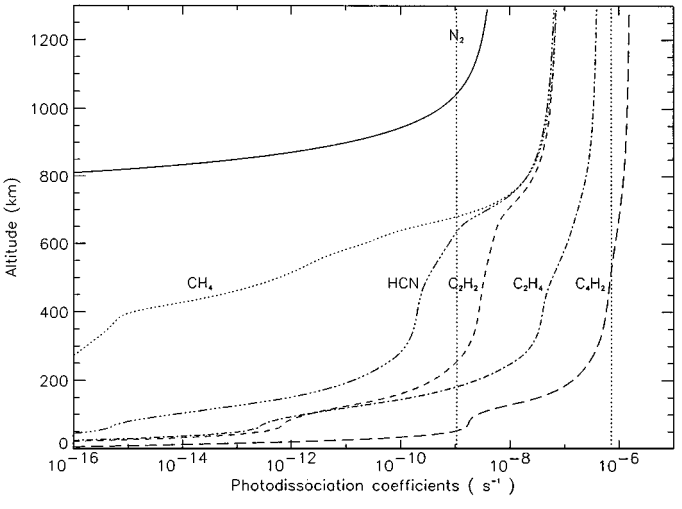

FIG. 2. Photodissociation coefficients of several compounds for spring equatorial conditions. The vertical dotted lines indicate the year timescale ($1/TY \sim 1 \times 10^{-9}$ s^{-1}) and the day timescale ($\sim 1 \times 10^{-6}$ s^{-1}).

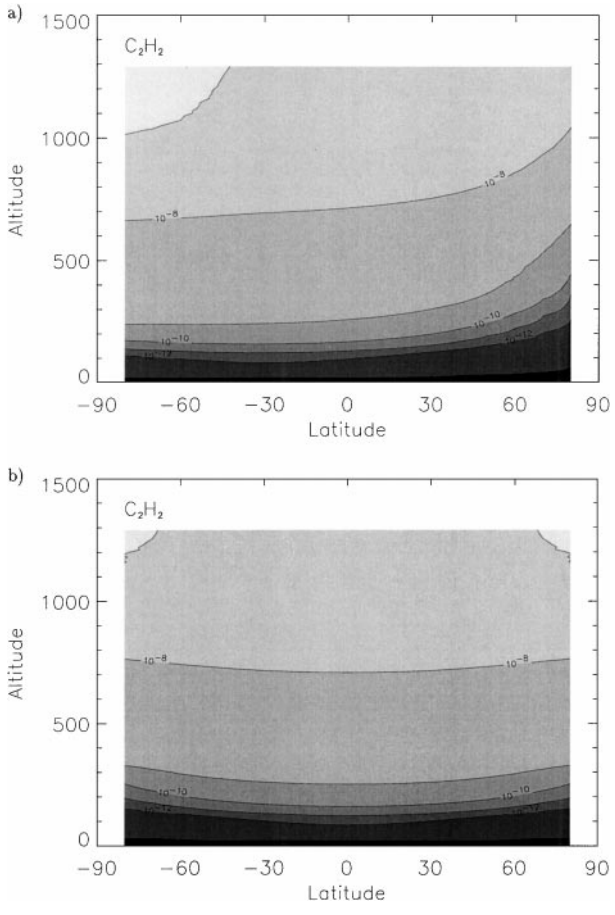

FIG. 3. Photodissociation coefficients of acetylene (s^{-1}) at (a) northern winter solstice and (b) spring equinox.

$$CH_4 + h\nu \xrightarrow{0.41} CH_3 + H$$
$$CH_4 + h\nu \xrightarrow{0.53} {}^1CH_2 + H_2$$
$$CH_4 + h\nu \xrightarrow{0.06} CH + H_2 + H$$

but found very similar results. The differences are only visible in the very high atmosphere ($z > 800$ km): with Smith and Raulin scheme, $^1CH_2$ is higher, and yields $^3CH_2$ (then CH) (R120, R100, R45) and CH_3 (R101). Though CH_3 is also higher, HCN (its main product at these altitudes (R220, R221 + R234)) keeps the same level for both schemes. CH also keeps the same level. For the molecules, only CH_2CCH_2 is enhanced in the high atmosphere, because of the enhancement of $^1CH_2$ (R105). The same conclusion can be drawn with the first scheme from Mordaunt *et al.* (1993):

$$CH_4 + h\nu \xrightarrow{0.51} CH_3 + H$$
$$CH_4 + h\nu \xrightarrow{0.24} {}^1CH_2 + H_2$$
$$CH_4 + h\nu \xrightarrow{0.25} {}^3CH_2 + 2H.$$

Another study by Wilson and Atreya has given similar results (Wilson and Atreya 1999).

Concerning the dissociation of N_2, we take the simplifying hypothesis that $N(^2D)$ atoms are rapidly quenched down to $N(^4S)$ atoms. This hypothesis does not yield any significant discrepancies with previous models. We also included dissociation of N_2 by cosmic rays with the dissociation profile from Lara *et al.* (1996), but this introduction had no significant impact on the atmospheric composition (except on N atoms). The chemistry of the metastable state $C_4H_2^*$ has been included as recommended by Zwier and Allen (1996). The chemical reactions presented in Tables IV and V were taken from previous models (Yung *et al.* 1984, Toublanc *et al.* 1995, Lara *et al.* 1996), from the litterature (references are given) and also from a recent study on hydrocarbons photochemistry (Smith 1999). For radicals C_2H, C_4H, and C_3N, some reactions have been estimated by analogy to others. Yung *et al.* (1984) suggested that the insertion of C_2H radicals on C_4H_2 molecules is similar to the insertion on C_2H_2 molecules, and that the C_4H radicals behave similarly, but are less reactive (factor 1/3 on reaction rates). Zwier and Allen (1996) also suggested that C_3N radicals are behaving the same way as C_2H radicals, and that the insertion on HC_3N molecules is similar to the insertion on $C_{2n}H_2$ molecules. We adopted these hypotheses to estimate several reactions. Concerning nitriles, the chemistry included is still to be improved. As in previous models, C_2N_2 is badly underestimated, and HC_3N seems overestimated by a factor of approximately 10. The excited state HC_3N^* has not been taken into account, but some preliminary studies show that its reactivity could be high, and that it could react in a similar way as $C_4H_2^*$ (Ferris *et al.* 1990; Zwier, private communication). CH_3CN was not introduced in this model, despite its detection in Titan's atmosphere (Bézard *et al.* 1993). The whole nitriles chemistry does not influence significantly the hydrocarbons composition, and it should be addressed in more detail in further studies, as well as the chemistry of oxygeneous compounds.

2.3. Transport

In one-dimensional models, eddy diffusion is used to account for the vertical transport of chemical species. The vertical profile of eddy diffusion coefficient must be tuned to reproduce observations (Hunten 1975). This one-dimensional representation fails to reproduce the latitudinal behavior of chemical species in the stratosphere of Titan as observed by Voyager I, even with a realistic representation of the seasonal and latitudinal variations of the UV field (Lebonnois and Toublanc 1999). The new aspect of the present work is to introduce a better modeling of the transport mechanisms in the lower atmosphere of Titan. Therefore, we introduced dynamical transport by meridional and vertical winds and by horizontal eddy diffusion. Vertical molecular and eddy diffusion are still taken into account.

Meridional winds. Rather than directly using the mean meridional winds from the GCM, we used an analytical

TABLE IV
Photodissociations

Photodissociations		Branching ratios	References
$CH_3 + h\nu$	$\xrightarrow{1}$ $^1CH_2 + H$	$\lambda = 216$ nm, $\sigma \sim 4.4 \times 10^{-17}$ cm^2	Arthur 1986
$CH_4 + h\nu$	$\xrightarrow{2}$ $^1CH_2 + H_2$	Lyα : 0.; other : 1	Mordaunt *et al.* 1993
$CH_4 + h\nu$	$\xrightarrow{3}$ $CH + H_2 + H$	Lyα : 0.51; other : 0	id.
$CH_4 + h\nu$	$\xrightarrow{4}$ $CH_3 + H$	Lyα : 0.49; other : 0	id.
$C_2H_2 + h\nu$	$\xrightarrow{5}$ $C_2H + H$	$\lambda < 150$ nm : 0.3; other : 0.08	Okabe 1983
$C_2H_2 + h\nu$	$\xrightarrow{6}$ $C_2 + H_2$	0.1	id.
$C_2H_4 + h\nu$	$\xrightarrow{7}$ $C_2H_2 + H_2$	0.51	Zelikoff *et al.* 1953 &
$C_2H_4 + h\nu$	$\xrightarrow{8}$ $C_2H_2 + 2\,H$	0.49	Back *et al.* 1967
$C_2H_6 + h\nu$	$\xrightarrow{9}$ $C_2H_4 + H_2$	Lyα : 0.13; other : 0.56	Lias *et al.* 1970
$C_2H_6 + h\nu$	$\xrightarrow{10}$ $C_2H_4 + 2\,H$	Lyα : 0.30; other : 0.14	id.
$C_2H_6 + h\nu$	$\xrightarrow{11}$ $C_2H_2 + 2\,H_2$	Lyα : 0.25; other : 0.27	id.
$C_2H_6 + h\nu$	$\xrightarrow{12}$ $CH_4 + {}^1CH_2$	Lyα : 0.25; other : 0.02	id.
$C_2H_6 + h\nu$	$\xrightarrow{13}$ $2\,CH_3$	Lyα : 0.08; other : 0.01	id.
$C_3H_3 + h\nu$	$\xrightarrow{14}$ $C_3H_2 + H$	$\lambda < 190$ nm, $\sigma \sim 4.0 \times 10^{-17}$ cm^2 (estimated)	Jackson *et al.* 1991
$CH_2CCH_2 + h\nu$	$\xrightarrow{15}$ $C_3H_3 + H$	0.89	id.
$CH_2CCH_2 + h\nu$	$\xrightarrow{16}$ $C_3H_2 + H_2$	0.11	id.
$CH_3C_2H + h\nu$	$\xrightarrow{17}$ $C_3H_3 + H$	0.89	id.
$CH_3C_2H + h\nu$	$\xrightarrow{18}$ $C_3H_2 + H_2$	0.11	id.
$C_3H_6 + h\nu$	$\xrightarrow{19}$ $CH_2CCH_2 + 2\,H$	0.33	Collin *et al.* 1979,
$C_3H_6 + h\nu$	$\xrightarrow{20}$ $CH_3C_2H + 2\,H$	0.17	Niedzielski *et al.* 1982 &
$C_3H_6 + h\nu$	$\xrightarrow{21}$ $C_2H_4 + {}^3CH_2$	0.03	Gierczak *et al.* 1988
$C_3H_6 + h\nu$	$\xrightarrow{22}$ $C_2H_3 + CH_3$	0.35	id.
$C_3H_6 + h\nu$	$\xrightarrow{23}$ $C_2H_2 + CH_4$	0.05	id.
$C_3H_8 + h\nu$	$\xrightarrow{24}$ $C_3H_6 + H_2$	Lyα : 0.33; other : 0.94	Calvert and Pitts 1966
$C_3H_8 + h\nu$	$\xrightarrow{25}$ $C_2H_6 + {}^1CH_2$	Lyα : 0.09; other : 0.	id.
$C_3H_8 + h\nu$	$\xrightarrow{26}$ $C_2H_5 + CH_3$	Lyα : 0.39; other : 0.	id.
$C_3H_8 + h\nu$	$\xrightarrow{27}$ $C_2H_4 + CH_4$	Lyα : 0.20; other : 0.06	id.
$C_4H_2 + h\nu$	$\xrightarrow{28}$ $C_4H + H$	$\lambda < 165$ nm : 0.2; other : 0	Glicker and Okabe 1987
$C_4H_2 + h\nu$	$\xrightarrow{29}$ $2\,C_2H$	$\lambda < 165$ nm : 0.03; $\lambda < 205$ nm : 0.01	id.
$C_4H_2 + h\nu$	$\xrightarrow{30}$ $C_2H_2 + C_2$	$\lambda < 165$ nm : 0.1; $\lambda < 205$ nm : 0.06	id.
$C_4H_2 + h\nu$	$\xrightarrow{31}$ $C_4H_2^*$	$\lambda < 165$ nm : 0.67; $\lambda < 205$ nm : 0.93; other : 1	id.
$C_4H_4 + h\nu$	$\xrightarrow{32}$ $C_4H_2 + H_2$	0.8	Gladstone *et al.* 1996
$C_4H_4 + h\nu$	$\xrightarrow{33}$ $2\,C_2H_2$	0.2	id.
$C_4H_6 + h\nu$	$\xrightarrow{34}$ $C_4H_4 + H_2$	0.04	Doepker 1968
$C_4H_6 + h\nu$	$\xrightarrow{35}$ $C_2H_4 + C_2H_2$	0.27	id.
$C_4H_6 + h\nu$	$\xrightarrow{36}$ $CH_3 + C_3H_3$	0.69	id.
$N_2 + h\nu$	$\xrightarrow{37}$ $2\,N(^4S)$		Okabe 1978
$HCN + h\nu$	$\xrightarrow{38}$ $H + CN$		Lee 1980
$HC_3N + h\nu$	$\xrightarrow{39}$ $C_2H + CN$	$\lambda < 150$ nm : 0.3; other : 0.05	Yung *et al.* 1984 & Clarke and Ferris 1995
$HC_3N + h\nu$	$\xrightarrow{40}$ $C_3N + H$	0.09	Clarke and Ferris 1995
$C_2N_2 + h\nu$	$\xrightarrow{41}$ $2\,CN$	0.3	Yung *et al.* 1984

reconstruction described in the Appendix. The stream functions at northern winter solstice and equinox for the reconstructed winds are plotted in Fig. 4. Figure 5 shows the quadratic means of the reconstructed meridional wind $\overline{v}$ (in m s^{-1}) and vertical wind $\overline{w}$ (in mm s^{-1}). The mean meridional circulation consists of a single pole-to-pole Hadley cell most of the year, with its ascending branch in the summer hemisphere (direct thermal cell). Around equinoxes, the ascending motion moves from one pole to the other, therefore creating two equator-to-pole Hadley cells. The GCM predicts much weaker winds around this reversal (a factor of 3 is used for the synthetic reconstruction).

TABLE V
Chemical Reactions

Reactions	Rates	References
$H + H + M \xrightarrow{42} H_2 + M$	$1.5 \times 10^{-29} T^{-1.3}$	Tsang and Hampson 1986
$H + CH \xrightarrow{43} H_2 + C$	$1.31 \times 10^{-10} e^{-80/T}$	Harding *et al.* 1993
$H + {}^1CH_2 \xrightarrow{44} CH + H_2$	$5. \times 10^{-11}$	Tsang and Hampson 1986
$H + {}^3CH_2 \xrightarrow{45} CH + H_2$	$3.54 \times 10^{-11} T^{0.32}$	Fulle and Hippler 1997
$H + CH_3 + M \xrightarrow{46} CH_4 + M$	$k_0 = 6.33 \times 10^{-21} T^{-2.98} e^{-635/T}$	Forst 1991
	$k_\infty = 2.63 \times 10^{-8} T^{-0.6} e^{-189/T}$	
$H + CH_3 \xrightarrow{47} H_2 + {}^3CH_2$	$1. \times 10^{-10} e^{-7600/T}$	Baulch *et al.* 1992
$H + CH_4 \xrightarrow{48} H_2 + CH_3$	$2.18 \times 10^{-20} T^3 \cdot e^{-4045/T}$	id.
$H + C_2H \xrightarrow{49} C_2H_2$	$3. \times 10^{-10}$	Tsang and Hampson 1986
$H + C_2H_2 + M \xrightarrow{50} C_2H_3 + M$	$k_0 = 3.3 \times 10^{-30} e^{-740/T}$	Baulch *et al.* 1992
	$k_\infty = 1.4 \times 10^{-11} e^{-1300/T}$	
$H + C_2H_3 \xrightarrow{51} H_2 + C_2H_2$	$6.86 \times 10^{-11} e^{23/T}$	Monks *et al.* 1995
$H + C_2H_3 + M \xrightarrow{52} C_2H_4 + M$	$k_0 = 5.76 \times 10^{-24} T^{-1.3}$	Monks *et al.* 1995 &
	$k_\infty = 8.9 \times 10^{-10} e^{-494/T}$	Duran *et al.* 1988
$H + C_2H_4 + M \xrightarrow{53} C_2H_5 + M$	$k_0 = 1.39 \times 10^{-29} e^{-562/T}$	Baulch *et al.* 1994
	$k_\infty = 6.6 \times 10^{-15} T^{1.28} e^{-650/T}$	
$H + C_2H_5 \xrightarrow{54} 2\ CH_3$	$7.95 \times 10^{-11} e^{-127/T}$	Pratt *et al.* 1984
$H + C_2H_5 \xrightarrow{55} H_2 + C_2H_4$	$3. \times 10^{-12}$	Tsang and Hampson 1986
$H + C_2H_5 + M \xrightarrow{56} C_2H_6 + M$	$k_0 = 5.5 \times 10^{-23} T^{-2} \cdot e^{-1040/T}$	Teng and Jones 1972 &
	$k_\infty = 1.66 \times 10^{-10}$	Sillesen *et al.* 1993
$H + C_2H_6 \xrightarrow{57} H_2 + C_2H_5$	$2.4 \times 10^{-15} T^{1.5} e^{-3730/T}$	Baulch *et al.* 1992
$H + C_3H_2 \xrightarrow{58} C_3H_3$	7.21×10^{-11}	Homann and Wellmann 1983
$H + C_3H_3 \xrightarrow{59} CH_3C_2H$	7.21×10^{-11}	id.
$H + CH_2CCH_2 \xrightarrow{60} C_3H_5$	$1.4 \times 10^{-11} e^{-1005/T}$	Wagner and Zellner 1972b
$H + CH_3C_2H \xrightarrow{61} C_3H_5$	$1.1 \times 10^{-11} e^{-1005/T}$	Wagner and Zellner 1972a
$H + CH_3C_2H \xrightarrow{62} CH_3 + C_2H_2$	$9.6 \times 10^{-12} e^{-1560/T}$	id.
$H + C_3H_5 \xrightarrow{63} CH_2CCH_2 + H_2$	1.4×10^{-11}	Hanning-Lee and Pilling 1992
$H + C_3H_5 \xrightarrow{64} CH_3C_2H + H_2$	1.4×10^{-11}	id.
$H + C_3H_5 \xrightarrow{65} C_3H_6$	2.8×10^{-10}	id.
$H + C_3H_6 \xrightarrow{66} C_3H_5 + H_2$	$2.87 \times 10^{-19} T^{2.5} e^{-1254/T}$	Tsang 1991
$H + C_3H_6 \xrightarrow{67} C_2H_4 + CH_3$	$4.31 \times 10^{-16} T^{1.5} e^{-1006/T}$	Hidaka *et al.* 1992
$H + C_3H_6 \xrightarrow{68} C_3H_7$	$1.2 \times 10^{-11} e^{-1460/T}$	id.
$H + C_3H_7 \xrightarrow{69} C_3H_6 + H_2$	$3. \times 10^{-12}$	Tsang 1988
$H + C_3H_8 \xrightarrow{70} C_3H_7 + H_2$	$2.2 \times 10^{-18} T^{2.54} e^{-3400/T}$	id.
$H + C_4H_2 \xrightarrow{71} C_4H_3$	$1.39 \times 10^{-10} e^{-1184/T}$	Nava *et al.* 1986
$H + C_4H_3 \xrightarrow{72} C_4H_4$	$8.56 \times 10^{-10} e^{-405/T}$	Schwanebeck and Warnatz 1975 & Duran *et al.* 1988
$H + C_4H_3 \xrightarrow{73} C_4H_2 + H_2$	1.2×10^{-11}	Schwanebeck and Warnatz 1975
$H + C_4H_3 \xrightarrow{74} 2\ C_2H_2$	3.3×10^{-12}	id.
$H_2 + C + M \xrightarrow{75} {}^3CH_2 + M$	$k_0 = 6.89 \times 10^{-32}$	Husain and Young 1975 &
	$k_\infty = 2.06 \times 10^{-11} e^{-57/T}$	Harding *et al.* 1993
$H_2 + CH + M \xrightarrow{76} CH_3 + M$	$k_0 = 1.5 \times 10^{-23} T^{-2.6}$	Fulle and Hippler 1997
	$k_\infty = 8.55 \times 10^{-11} T^{0.15}$	
$H_2 + CH \xrightarrow{77} {}^3CH_2 + H$	$3.10 \times 10^{-10} e^{-1650/T}$	Brownsword *et al.* 1997
$H_2 + {}^1CH_2 \xrightarrow{78} CH_3 + H$	1.2×10^{-10}	Tsang and Hampson 1986
$H_2 + CH_3 \xrightarrow{79} CH_4 + H$	$1.14 \times 10^{-20} T^{2.74} e^{-4740/T}$	Baulch *et al.* 1992
$H_2 + C_2 \xrightarrow{80} C_2H_2$	$1.77 \times 10^{-10} e^{-1470/T}$	Pitts *et al.* 1982
$H_2 + C_2H \xrightarrow{81} C_2H_2 + H$	$1.2 \times 10^{-11} e^{-998/T}$	Opansky and Leone 1996b
$H_2 + C_2H_3 \xrightarrow{82} C_2H_4 + H$	$1.57 \times 10^{-20} T^{2.56} e^{-2529/T}$	Knyazev *et al.* 1996
$H_2 + C_2H_5 \xrightarrow{83} C_2H_6 + H$	$5.11 \times 10^{-24} T^{3.6} e^{-4253/T}$	Tsang and Hampson 1986
$H_2 + C_3H_5 \xrightarrow{84} C_3H_6 + H$	$1.8 \times 10^{-19} T^{2.38} e^{-9557/T}$	Tsang 1991

TABLE V—*Continued*

Reactions	Rates	References
$H_2 + C_3H_7 \xrightarrow{85} C_3H_8 + H$	$3. \times 10^{-21} T^{2.84} e^{-4600/T}$	Tsang 1988
$C + C + M \xrightarrow{86} C_2 + M$	$k_0 = 4.97 \times 10^{-27} T^{-1.6}$	Slack 1976
	$k_\infty = 2.16 \times 10^{-11}$	Martinotti *et al.* 1968
$C + CH_4 \xrightarrow{87} C_2H_4$	$2. \times 10^{-15}$	Husain and Kirsch 1971
$C + C_2H_2 \xrightarrow{88} C_3H_2$	5.95×10^{-10}	Liao and Herbst 1995
$C + C_2H_4 \xrightarrow{89} CH_2CCH_2$	2.0×10^{-10}	Haider and Husain 1993
$C + CH_3C_2H \xrightarrow{90} C_4H_4$	3.9×10^{-10}	Haider and Husain 1992
$C + C_4H_6 \xrightarrow{91} C_3H_3 + C_2H_3$	1.1×10^{-9}	Husain and Ioannou 1997
$CH + CH \xrightarrow{92} C_2H_2$	1.99×10^{-10}	Braun *et al.* 1967
$CH + CH_4 \xrightarrow{93} C_2H_4 + H$	$3.96 \times 10^{-8} T^{-1.04} e^{-36/T}$	Canosa *et al.* 1997
$CH + C_2H_2 \xrightarrow{94} C_3H_3$	$1.59 \times 10^{-9} T^{-0.23} e^{-16/T}$	id.
$CH + C_2H_4 \xrightarrow{95} C_3H_5$	$7.75 \times 10^{-9} T^{-0.55} e^{-29/T}$	id.
$CH + C_2H_6 \xrightarrow{96} C_3H_7$	$3.8 \times 10^{-8} T^{-0.86} e^{-53/T}$	id.
$^1CH_2 + {}^1CH_2 \xrightarrow{97} C_2H_2 + 2\,H$	$5. \times 10^{-11}$	Tsang and Hampson 1986
$^1CH_2 + {}^3CH_2 \xrightarrow{98} C_2H_2 + 2\,H$	$3. \times 10^{-11}$	id.
$^1CH_2 + CH_3 \xrightarrow{99} C_2H_4 + H$	$3. \times 10^{-11}$	id.
$^1CH_2 + CH_4 \xrightarrow{100} {}^3CH_2 + CH_4$	1.2×10^{-11}	Böhland *et al.* 1985a
$^1CH_2 + CH_4 \xrightarrow{101} 2\,CH_3$	5.9×10^{-11}	id.
$^1CH_2 + C_2H \xrightarrow{102} C_2H_2 + CH$	$3. \times 10^{-11}$	Tsang and Hampson 1986
$^1CH_2 + C_2H_2 \xrightarrow{103} {}^3CH_2 + C_2H_2$	8.14×10^{-11}	Baulch *et al.* 1992
$^1CH_2 + C_2H_2 \xrightarrow{104} C_3H_3 + H$	9.62×10^{-11}	id.
$^1CH_2 + C_2H_2 \xrightarrow{105} CH_2CCH_2$	9.62×10^{-11}	id.
$^1CH_2 + C_2H_2 \xrightarrow{106} CH_3C_2H$	9.62×10^{-11}	id.
$^1CH_2 + C_2H_3 \xrightarrow{107} C_2H_2 + CH_3$	$3. \times 10^{-11}$	Tsang and Hampson 1986
$^1CH_2 + C_2H_4 \xrightarrow{108} {}^3CH_2 + C_2H_4$	2.3×10^{-11}	Baulch *et al.* 1992
$^1CH_2 + C_2H_4 \xrightarrow{109} C_3H_6$	1.5×10^{-10}	id.
$^1CH_2 + C_2H_5 \xrightarrow{110} C_2H_4 + CH_3$	1.5×10^{-11}	Tsang and Hampson 1986
$^1CH_2 + C_2H_5 \xrightarrow{111} C_3H_6 + H$	1.5×10^{-11}	id.
$^1CH_2 + C_2H_6 \xrightarrow{112} {}^3CH_2 + C_2H_6$	3.6×10^{-11}	Baulch *et al.* 1992
$^1CH_2 + C_2H_6 \xrightarrow{113} C_2H_5 + CH_3$	1.9×10^{-10}	Tsang and Hampson 1986
$^1CH_2 + C_3H_5 \xrightarrow{114} C_4H_6 + H$	3.3×10^{-10}	Tsang 1991
$^1CH_2 + C_3H_5 \xrightarrow{115} C_2H_4 + C_2H_3$	6.67×10^{-11}	id.
$^1CH_2 + C_3H_6 \xrightarrow{116} C_3H_5 + CH_3$	8.7×10^{-11}	id.
$^1CH_2 + C_3H_7 \xrightarrow{117} C_2H_5 + C_2H_4$	4.29×10^{-11}	Tsang 1988
$^1CH_2 + C_3H_7 \xrightarrow{118} C_3H_6 + CH_3$	1.71×10^{-11}	id.
$^1CH_2 + C_3H_8 \xrightarrow{119} 2\,C_2H_5$	1.6×10^{-10}	id.
$^1CH_2 + N_2 \xrightarrow{120} {}^3CH_2 + N_2$	$1. \times 10^{-11}$	Baulch *et al.* 1992
$^3CH_2 + {}^3CH_2 \xrightarrow{121} C_2H_2 + 2\,H$	$1.8 \times 10^{-10} e^{-400/T}$	id.
$^3CH_2 + CH_3 \xrightarrow{122} C_2H_4 + H$	$7. \times 10^{-11}$	id.
$^3CH_2 + CH_4 \xrightarrow{123} 2\,CH_3$	$7.13 \times 10^{-12} e^{-5052/T}$	Böhland *et al.* 1985b
$^3CH_2 + CH_4 \xrightarrow{124} C_2H_6$	$3.5 \times 10^{-12} e^{-3332/T}$	id.
$^3CH_2 + C_2H \xrightarrow{125} C_2H_2 + CH$	$3. \times 10^{-11}$	Tsang and Hampson 1986
$^3CH_2 + C_2H_2 \xrightarrow{126} CH_3C_2H$	$1. \times 10^{-11} e^{-3330/T}$	Baulch *et al.* 1992
$^3CH_2 + C_2H_2 \xrightarrow{127} CH_2CCH_2$	$1. \times 10^{-11} e^{-3330/T}$	id.
$^3CH_2 + C_2H_3 \xrightarrow{128} C_2H_2 + CH_3$	$3. \times 10^{-11}$	Tsang and Hampson 1986
$^3CH_2 + C_2H_4 \xrightarrow{129} C_3H_6$	$5.31 \times 10^{-12} e^{-2658/T}$	Kraus *et al.* 1993
$^3CH_2 + C_2H_5 \xrightarrow{130} C_2H_4 + CH_3$	$3. \times 10^{-11}$	Tsang and Hampson 1986
$^3CH_2 + C_2H_6 \xrightarrow{131} C_3H_8$	$8.13 \times 10^{-12} e^{-3332/T}$	Böhland *et al.* 1985b
$^3CH_2 + C_2H_6 \xrightarrow{132} C_2H_5 + CH_3$	$1.07 \times 10^{-11} e^{-3981/T}$	id.

TABLE V—*Continued*

Reactions	Rates	References
$^3CH_2 + C_3H_5 \xrightarrow{133} C_4H_6 + H$	$5. \times 10^{-11}$	Tsang 1991
$^3CH_2 + C_3H_6 \xrightarrow{134} C_3H_5 + CH_3$	$1.2 \times 10^{-12} e^{-3116/T}$	id.
$^3CH_2 + C_3H_7 \xrightarrow{135} C_3H_6 + CH_3$	$3. \times 10^{-12}$	Tsang 1988
$^3CH_2 + C_3H_7 \xrightarrow{136} C_2H_4 + C_2H_5$	$3. \times 10^{-11}$	id.
$^3CH_2 + C_3H_8 \xrightarrow{137} C_4H_{10}$	$8.13 \times 10^{-12} e^{-3332/T}$	Böhland *et al.* 1985b
$^3CH_2 + C_3H_8 \xrightarrow{138} C_3H_7 + CH_3$	$1.5 \times 10^{-24} T^{3.65} e^{-3600/T}$	Tsang 1988
$^3CH_2 + C_4H_2 \xrightarrow{139} C_4H + CH_3$	$2.16 \times 10^{-11} e^{-2165/T}$	Böhland *et al.* 1988
$CH_3 + CH_3 \xrightarrow{140} C_2H_5 + H$	$8.28 \times 10^{-12} T^{0.1} e^{-5335/T}$	Stewart *et al.* 1989
$CH_3 + CH_3 + M \xrightarrow{141} C_2H_6 + M$	$k_0 = 1.7 \times 10^{-5} T^{-7.25} e^{-2172/T}$	Du *et al.* 1996
	$k_\infty = 1.53 \times 10^{-7} T^{-1.2} e^{-295/T}$	
$CH_3 + C_2H \xrightarrow{142} C_3H_3 + H$	$4. \times 10^{-11}$	Tsang and Hampson 1986
$CH_3 + C_2H_2 \xrightarrow{143} C_3H_5$	$1. \times 10^{-12} e^{-3877/T}$	id.
$CH_3 + C_2H_3 \xrightarrow{144} C_2H_2 + CH_4$	3.4×10^{-11}	Fahr *et al.* 1991
$CH_3 + C_2H_3 \xrightarrow{145} C_3H_6$	1.2×10^{-10}	id.
$CH_3 + C_2H_4 \xrightarrow{146} C_2H_3 + CH_4$	$1.1 \times 10^{-23} T^{3.7} e^{-4780/T}$	Tsang and Hampson 1986
$CH_3 + C_2H_4 \xrightarrow{147} C_3H_7$	$3.5 \times 10^{-13} e^{-3700/T}$	Baulch *et al.* 1992
$CH_3 + C_2H_5 \xrightarrow{148} C_2H_4 + CH_4$	$3.25 \times 10^{-11} T^{-0.5}$	Tsang and Hampson 1986
$CH_3 + C_2H_5 + M \xrightarrow{149} C_3H_8 + M$	$k_0 = 1.01 \times 10^{20} T^{-16.14} e^{-1897/T}$	Tsang and Hampson 1986 &
	$k_\infty = 8.12 \times 10^{-10} T^{-0.5}$	Laufer *et al.* 1983
$CH_3 + C_2H_6 \xrightarrow{150} C_2H_5 + CH_4$	$2.5 \times 10^{-31} T^{6.} e^{-3043/T}$	Baulch *et al.* 1992
$CH_3 + CH_3C_2H \xrightarrow{151} C_2H_6 + C_2H$	$8.32 \times 10^{-13} e^{-4428/T}$	Kerr and Parsonage 1972
$CH_3 + CH_2CCH_2 \xrightarrow{152} C_2H_5 + C_2H_2$	$3.32 \times 10^{-13} e^{-4076/T}$	id.
$CH_3 + C_3H_5 \xrightarrow{153} CH_2CCH_2 + CH_4$	$5. \times 10^{-12} T^{-0.32} e^{66/T}$	Tsang 1991
$CH_3 + C_3H_6 \xrightarrow{154} C_3H_5 + CH_4$	$2.66 \times 10^{-13} e^{-4440/T}$	Kinsman and Roscoe 1994
$CH_3 + C_3H_7 + M \xrightarrow{155} C_4H_{10} + M$	$k_0 = 8.63 \times 10^{28} T^{-18.5} e^{-2307/T}$	Laufer *et al.* 1983
	$k_\infty = 3.2 \times 10^{-10} T^{-0.32}$	
$CH_3 + C_3H_7 \xrightarrow{156} C_3H_6 + CH_4$	$1.9 \times 10^{-11} T^{-0.32}$	Tsang 1988
$CH_3 + C_3H_8 \xrightarrow{157} C_3H_7 + CH_4$	$1.5 \times 10^{-24} T^{3.65} e^{-3600/T}$	id.
$CH_3 + C_4H_4 \xrightarrow{158} C_4H_3 + CH_4$	$6.61 \times 10^{-13} e^{-2502/T}$	Scherzer *et al.* 1985
$CH_4 + C_2 \xrightarrow{159} C_2H + CH_3$	$5.05 \times 10^{-11} e^{-297/T}$	Pitts *et al.* 1982
$CH_4 + C_2H \xrightarrow{160} C_2H_2 + CH_3$	$1.2 \times 10^{-11} e^{-491/T}$	Opansky and Leone 1996a
$CH_4 + C_2H_3 \xrightarrow{161} C_2H_4 + CH_3$	$2.4 \times 10^{-24} T^{4.02} e^{-2754/T}$	Tsang and Hampson 1986
$CH_4 + C_2H_5 \xrightarrow{162} C_2H_6 + CH_3$	$1.43 \times 10^{-25} T^{4.14} e^{-6322/T}$	id.
$CH_4 + C_3H_7 \xrightarrow{163} C_3H_8 + CH_3$	$4. \times 10^{-26} T^{4.02} e^{-5473/T}$	Tsang 1988
$C_2H + C_2H \xrightarrow{164} C_2H_2 + C_2$	$3. \times 10^{-12}$	Tsang and Hampson 1986
$C_2H + C_2H_2 \xrightarrow{165} C_4H_2 + H$	$8.6 \times 10^{-16} T^{1.8} e^{474/T}$	Opansky and Leone 1996a
$C_2H + C_2H_3 \xrightarrow{166} 2\,C_2H_2$	1.6×10^{-12}	Tsang and Hampson 1986
$C_2H + C_2H_4 \xrightarrow{167} C_4H_4 + H$	$7.8 \times 10^{-11} e^{134/T}$	Opansky and Leone 1996b
$C_2H + C_2H_5 \xrightarrow{168} C_3H_3 + CH_3$	$3. \times 10^{-11}$	Tsang and Hampson 1986
$C_2H + C_2H_5 \xrightarrow{169} C_2H_2 + C_2H_4$	$3. \times 10^{-12}$	id.
$C_2H + C_2H_6 \xrightarrow{170} C_2H_2 + C_2H_5$	$3.5 \times 10^{-11} e^{2/T}$	Opansky and Leone 1996b
$C_2H + C_3H_5 \xrightarrow{171} CH_2CCH_2 + C_2H_2$	1.2×10^{-11}	Tsang 1991
$C_2H + C_3H_6 \xrightarrow{172} CH_3C_2H + C_2H_3$	$2. \times 10^{-11}$	id.
$C_2H + C_3H_6 \xrightarrow{173} C_3H_5 + C_2H_2$	$6. \times 10^{-12}$	id.
$C_2H + C_3H_7 \xrightarrow{174} C_3H_3 + C_2H_5$	$2. \times 10^{-11}$	Tsang 1988
$C_2H + C_3H_7 \xrightarrow{175} C_3H_6 + C_2H_2$	$1. \times 10^{-11}$	id.
$C_2H + C_3H_8 \xrightarrow{176} C_3H_7 + C_2H_2$	$7.8 \times 10^{-11} e^{3/T}$	Hoobler *et al.* 1997
$C_2H_2 + C_2H_3 \xrightarrow{177} C_4H_4 + H$	$3.32 \times 10^{-12} e^{-2516/T}$	Fahr and Stein 1989
$C_2H_2 + C_3H_2 \xrightarrow{178} C_4H_2 + {}^3CH_2$	$5. \times 10^{-13}$	Homann and Schweinfurth 1981

TABLE V—*Continued*

Reactions		Rates	References
$C_2H_2 + C_3H_3$	$\xrightarrow{179}$ $C_4H_2 + CH_3$	$2. \times 10^{-13}$	id.
$C_2H_2 + C_3H_7$	$\xrightarrow{180}$ $C_2H_4 + C_3H_5$	$1.2 \times 10^{-12} e^{-4531/T}$	Tsang 1988
$C_2H_3 + C_2H_3$	$\xrightarrow{181}$ C_4H_6	1.2×10^{-10}	Fahr *et al.* 1991
$C_2H_3 + C_2H_3$	$\xrightarrow{182}$ $C_2H_2 + C_2H_4$	2.4×10^{-11}	id.
$C_2H_3 + C_2H_4$	$\xrightarrow{183}$ $C_4H_6 + H$	$8.3 \times 10^{-13} e^{-3676/T}$	Tsang and Hampson 1986
$C_2H_3 + C_2H_5$	$\xrightarrow{184}$ $C_3H_5 + CH_3$	$6.1 \times 10^{-47} T^{11.25} e^{3289/T}$	id.
$C_2H_3 + C_2H_5$	$\xrightarrow{185}$ $2\ C_2H_4$	$8. \times 10^{-13}$	id.
$C_2H_3 + C_2H_5$	$\xrightarrow{186}$ $C_2H_2 + C_2H_6$	$8. \times 10^{-13}$	id.
$C_2H_3 + C_2H_6$	$\xrightarrow{187}$ $C_2H_4 + C_2H_5$	$9.98 \times 10^{-22} T^{3.3} e^{-5285/T}$	id.
$C_2H_3 + C_3H_5$	$\xrightarrow{188}$ $CH_2CCH_2 + C_2H_4$	$4. \times 10^{-12}$	Tsang 1991
$C_2H_3 + C_3H_5$	$\xrightarrow{189}$ $C_3H_6 + C_2H_2$	$8. \times 10^{-12}$	id.
$C_2H_3 + C_3H_6$	$\xrightarrow{190}$ $C_4H_6 + CH_3$	$1.2 \times 10^{-12} e^{-2520/T}$	id.
$C_2H_3 + C_3H_6$	$\xrightarrow{191}$ $C_3H_5 + C_2H_4$	$3.68 \times 10^{-24} T^{3.5} e^{-2356/T}$	id.
$C_2H_3 + C_3H_7$	$\xrightarrow{192}$ $C_3H_6 + C_2H_4$	$2. \times 10^{-12}$	Tsang 1988
$C_2H_3 + C_3H_7$	$\xrightarrow{193}$ $C_3H_8 + C_2H_2$	$2. \times 10^{-12}$	id.
$C_2H_3 + C_3H_8$	$\xrightarrow{194}$ $C_3H_7 + C_2H_4$	$1. \times 10^{-21} T^{3.3} e^{-5285/T}$	id.
$C_2H_4 + C_2H_5$	$\xrightarrow{195}$ $C_2H_6 + C_2H_3$	$1. \times 10^{-21} T^{3.13} e^{-9063/T}$	Tsang and Hampson 1986
$C_2H_5 + C_2H_5 + M$	$\xrightarrow{196}$ $C_4H_{10} + M$	$k_0 = 6.59 \times 10^{-6} T^{-6.39} e^{-301/T}$ $k_\infty = 1.26 \times 10^{-11} e^{-96/T}$	Laufer *et al.* 1983
$C_2H_5 + C_2H_5$	$\xrightarrow{197}$ $C_2H_6 + C_2H_4$	$2.74 \times 10^{-11} e^{-402/T}$	Ivin and Steacie 1951
$C_2H_5 + C_3H_5$	$\xrightarrow{198}$ $CH_2CCH_2 + C_2H_6$	$1.6 \times 10^{-12} e^{66/T}$	Tsang 1991
$C_2H_5 + C_3H_5$	$\xrightarrow{199}$ $C_3H_6 + C_2H_4$	$4.3 \times 10^{-12} e^{66/T}$	id.
$C_2H_5 + C_3H_6$	$\xrightarrow{200}$ $C_2H_6 + C_3H_5$	$3.7 \times 10^{-24} T^{3.5} e^{-3340/T}$	id.
$C_2H_5 + C_3H_7$	$\xrightarrow{201}$ $C_3H_6 + C_2H_6$	2.4×10^{-12}	Tsang 1988
$C_2H_5 + C_3H_7$	$\xrightarrow{202}$ $C_3H_8 + C_2H_4$	1.9×10^{-12}	id.
$C_2H_5 + C_3H_8$	$\xrightarrow{203}$ $C_2H_6 + C_3H_7$	$1.5 \times 10^{-24} T^{3.65} e^{-4600/T}$	id.
$C_2H_6 + C_3H_5$	$\xrightarrow{204}$ $C_3H_6 + C_2H_5$	$3.9 \times 10^{-22} T^{3.3} e^{-9986/T}$	Tsang 1991
$C_2H_6 + C_3H_7$	$\xrightarrow{205}$ $C_3H_8 + C_2H_5$	$4.2 \times 10^{-25} T^{3.82} e^{-4550/T}$	Tsang 1988
$C_3H_5 + C_3H_5$	$\xrightarrow{206}$ $CH_2CCH_2 + C_3H_6$	$1.4 \times 10^{-13} e^{132/T}$	Tsang 1991
$C_3H_5 + C_3H_7$	$\xrightarrow{207}$ $2\ C_3H_6$	$2.4 \times 10^{-12} e^{66/T}$	id.
$C_3H_5 + C_3H_7$	$\xrightarrow{208}$ $CH_2CCH_2 + C_3H_8$	$1.2 \times 10^{-12} e^{66/T}$	id.
$C_3H_5 + C_3H_8$	$\xrightarrow{209}$ $C_3H_6 + C_3H_7$	$3.9 \times 10^{-22} T^{3.3} e^{-9986/T}$	id.
$C_3H_6 + C_3H_7$	$\xrightarrow{210}$ $C_3H_8 + C_3H_5$	$3.7 \times 10^{-24} T^{3.5} e^{-3340/T}$	id.
$C_3H_7 + C_3H_7$	$\xrightarrow{211}$ $C_3H_8 + C_3H_6$	2.8×10^{-12}	Tsang 1988
$C_4H_2^*$	$\xrightarrow{212}$ C_4H_2	upper limit : 1000 s^{-1}	Lisy and Klemperer 1980 & Zwier and Allen 1996
$C_4H_2^* + N_2$	$\xrightarrow{213}$ $C_4H_2 + N_2$	upper limit : 1.4×10^{-15}	Zwier and Allen 1996
N_2	$\xrightarrow{214}$ $2\ N(^4S)$	$1. \times 10^{-16}$ s^{-1} (GCR, 100–800 km)	Lara *et al.* 1996
$N(^4S) + H + M$	$\xrightarrow{215}$ $NH + M$	$5. \times 10^{-32}$	Brown 1973
$N(^4S) + C + M$	$\xrightarrow{216}$ $CN + M$	9.41×10^{-33}	Kley *et al.* 1974
$N(^4S) + CH$	$\xrightarrow{217}$ $CN + H$	$2.67 \times 10^{-10} T^{-0.09}$	Brownsword *et al.* 1996
$N(^4S) + N(^4S) + M$	$\xrightarrow{218}$ $N_2 + M$	$8.27 \times 10^{-34} e^{490/T}$	Campbell and Thrush 1967
$N(^4S) + CN$	$\xrightarrow{219}$ $N_2 + C$	$3.24 \times 10^{-13} e^{1770/T}$	Atakan and Wolfrum 1992
$N(^4S) + CH_3$	$\xrightarrow{220}$ $HCN + H_2$	$6. \times 10^{-12}$	Marston *et al.* 1989
$N(^4S) + CH_3$	$\xrightarrow{221}$ $H_2CN + H$	5.6×10^{-11}	id.
$N(^4S) + H_2CN$	$\xrightarrow{222}$ $HCN + NH$	$1. \times 10^{-10} e^{-200/T}$	Nesbitt *et al.* 1990
$N(^4S) + C_2N$	$\xrightarrow{223}$ $2\ CN$	$1. \times 10^{-10}$	Whyte and Phillips 1983
$NH + NH$	$\xrightarrow{224}$ $N_2 + 2\ H$	1.16×10^{-9}	Meaburn and Gordon 1968

TABLE V—*Continued*

Reactions		Rates	References
$CN + H_2$	$\xrightarrow{225}$ $HCN + H$	$2.23 \times 10^{-21} T^{3.31} e^{-756/T}$	Sun *et al.* 1990
$CN + CH_4$	$\xrightarrow{226}$ $HCN + CH_3$	$5.15 \times 10^{-16} T^{1.53} e^{-504/T}$	Yang *et al.* 1993
$CN + C_2H_2$	$\xrightarrow{227}$ $HC_3N + H$	$5.67 \times 10^{-9} T^{-0.55} e^{-4/T}$	Yang *et al.* 1992b
$CN + C_2H_4$	$\xrightarrow{228}$ $HCN + C_2H_3$	$3.66 \times 10^{-12} T^{0.7} e^{-28/T}$	Sims *et al.* 1993 & Monks *et al.* 1993
$CN + C_2H_6$	$\xrightarrow{229}$ $HCN + C_2H_5$	$5.91 \times 10^{-12} T^{0.22} e^{58/T}$	Sims *et al.* 1993
$CN + C_3H_8$	$\xrightarrow{230}$ $HCN + C_3H_7$	$3.58 \times 10^{-15} T^{1.14} e^{284/T}$	Hess *et al.* 1989
$CN + HCN$	$\xrightarrow{231}$ $C_2N_2 + H$	$6.31 \times 10^{-17} T^{1.57} e^{-50/T}$	Zabarnick and Lin 1989
$HCN + H + M$	$\xrightarrow{232}$ $H_2CN + M$	$k_0 = 4.4 \times 10^{-24} T^{-2.73} e^{-3855/T}$ $k_\infty = 5.5 \times 10^{-11} e^{-2438/T}$	Tsang 1991
$HCN + C_2H$	$\xrightarrow{233}$ $HC_3N + H$	$5.26 \times 10^{-12} e^{-770/T}$	Hoobler and Leone 1997
$H_2CN + H$	$\xrightarrow{234}$ $HCN + H_2$	$1.4 \times 10^{-10} e^{-200/T}$	Nesbitt *et al.* 1990
$C_2N_2 + C$	$\xrightarrow{235}$ $C_2N + CN$	$3. \times 10^{-11}$	Whyte and Phillips 1983
$C_3N + H_2$	$\xrightarrow{236}$ $HC_3N + H$	$1.2 \times 10^{-11} e^{-998/T}$	estimated, $k(C_2H + H_2)$
$C_3N + CH_4$	$\xrightarrow{237}$ $HC_3N + CH_3$	$1.2 \times 10^{-11} e^{-491/T}$	estimated, $k(C_2H + CH_4)$
$C_3N + C_2H_6$	$\xrightarrow{238}$ $HC_3N + C_2H_5$	$3.5 \times 10^{-11} e^{2/T}$	estimated, $k(C_2H + C_2H_6)$
$C_3N + C_3H_8$	$\xrightarrow{239}$ $HC_3N + C_3H_7$	6×10^{-12}	estimated, $k(C_2H + C_3H_8)$
$C_2H_3 + C_2H_5$	$\xrightarrow{240}$ soot	2.5×10^{-11}	Tsang and Hampson 1986
$CH_3C_2H + CH$	$\xrightarrow{241}$ soot	4.6×10^{-10}	Butler *et al.* 1981
$C_3H_5 + CH_3$	$\xrightarrow{242}$ soot	$1.69 \times 10^{-10} T^{-0.32} e^{66/T}$	Tsang 1991
$C_3H_5 + C_2H_2$	$\xrightarrow{243}$ soot	$5.3 \times 10^{-14} e^{-3500/T}$	id.
$C_3H_5 + C_2H_4$	$\xrightarrow{244}$ soot	$1. \times 10^{-14} e^{-5776/T}$	id.
$C_3H_5 + C_3H_5$	$\xrightarrow{245}$ soot	$1.7 \times 10^{-11} e^{132/T}$	id.
$C_3H_5 + C_3H_6$	$\xrightarrow{246}$ soot	$1. \times 10^{-14} e^{-5776/T}$	id.
$C_3H_5 + C_3H_7$	$\xrightarrow{247}$ soot	$3.4 \times 10^{-11} e^{66/T}$	id.
$C_3H_6 + CH_3$	$\xrightarrow{248}$ soot	$1.19 \times 10^{-13} e^{-3260/T}$	Kinsman and Roscoe 1994
$C_3H_6 + C_2H_3$	$\xrightarrow{249}$ soot	$1.2 \times 10^{-12} e^{-3240/T}$	Tsang 1991
$C_3H_7 + C_2H_3$	$\xrightarrow{250}$ soot	1.6×10^{-11}	Tsang 1988
$C_3H_7 + C_2H_4$	$\xrightarrow{251}$ soot	$3.24 \times 10^{-14} e^{-3070/T}$	Kerr and Parsonage 1972
$C_3H_7 + C_2H_5$	$\xrightarrow{252}$ soot	3.3×10^{-11}	Tsang 1988
$C_3H_7 + C_3H_7$	$\xrightarrow{253}$ soot	1.7×10^{-11}	id.
$C_3H_8 + CH$	$\xrightarrow{254}$ soot + H	$1.9 \times 10^{-10} e^{240/T}$	Baulch *et al.* 1992
$C_4H + C_2H_2$	$\xrightarrow{255}$ soot + H	$2.9 \times 10^{-16} T^{1.8} e^{474/T}$	estimated, $k(C_2H + C_2H_2)/3$
$C_4H_2 + C_2H$	$\xrightarrow{256}$ soot + H	$8.6 \times 10^{-16} T^{1.8} e^{474/T}$	estimated, $k(C_2H + C_2H_2)$
$C_4H_2 + C_4H$	$\xrightarrow{257}$ soot + H	$2.9 \times 10^{-16} T^{1.8} e^{474/T}$	estimated, $k(C_2H + C_2H_2)/3$
$C_4H_2^* + C_2H_2$	$\xrightarrow{258}$ soot + 2 H	3.5×10^{-13}	Zwier and Allen 1996
$C_4H_2^* + C_2H_4$	$\xrightarrow{259}$ soot + 2 H	4.2×10^{-13}	id.
$C_4H_2^* + CH_3C_2H$	$\xrightarrow{260}$ soot + 2 H	1.6×10^{-13}	id.
$C_4H_2^* + CH_3C_2H$	$\xrightarrow{261}$ soot + CH_3 + H	2.3×10^{-13}	id.
$C_4H_2^* + CH_3C_2H$	$\xrightarrow{262}$ soot + C_2H_2	2.5×10^{-13}	id.
$C_4H_2^* + CH_3C_2H$	$\xrightarrow{263}$ soot + C_2H_3	8.7×10^{-14}	id.
$C_4H_2^* + C_3H_6$	$\xrightarrow{264}$ soot + 2 H	1.6×10^{-13}	id.
$C_4H_2^* + C_3H_6$	$\xrightarrow{265}$ soot + CH_3 + H	4.1×10^{-13}	id.
$C_4H_2^* + C_3H_6$	$\xrightarrow{266}$ soot + C_2H_2	2.5×10^{-13}	id.
$C_4H_2^* + C_3H_6$	$\xrightarrow{267}$ soot + C_2H_3	4.9×10^{-14}	id.
$C_4H_2^* + C_4H_2$	$\xrightarrow{268}$ soot + 2 H	$1. \times 10^{-12}$	id.
$C_4H_2^* + C_4H_2$	$\xrightarrow{269}$ soot + C_2H_2	8.2×10^{-13}	id.
$C_4H_4 + C_4H_4$	$\xrightarrow{270}$ soot	$7.25 \times 10^{-14} e^{-9261/T}$	Lungard and Heicklen 1984

TABLE V—*Continued*

Reactions	Rates	References
$C_4H_6 + CH_3 \xrightarrow{271}$ soot	$1.35 \times 10^{-13} e^{-2063/T}$	Kerr and Parsonage 1972
$C_4H_6 + C_2H_3 \xrightarrow{272}$ soot	$2.45 \times 10^{-12} T^{-0.17} e^{-1630/T}$	Westmoreland *et al.* 1989
$C_4H_{10} + CH \xrightarrow{273}$ soot	$4.4 \times 10^{-10} e^{28/T}$	Baulch *et al.* 1992
$C_4H_{10} + {}^3CH_2 \xrightarrow{274}$ soot	4.3×10^{-12}	Halberstadt and Crump 1973
$N({}^4S) + C_2H_6 \xrightarrow{275}$ soot	$4. \times 10^{-16}$	Aleksandrov *et al.* 1990
$CN + C_2H_4 \xrightarrow{276}$ soot + H	$9.14 \times 10^{-13} T^{0.7} e^{-28/T}$	Sims *et al.* 1993 & Monks *et al.* 1993
$CN + C_2N_2 \xrightarrow{277}$ soot	$2.19 \times 10^{-21} T^{2.7} e^{-325/T}$	Yang *et al.* 1992a
$HCN + C_2H_3 \xrightarrow{278}$ soot + H	$1. \times 10^{-12} e^{-900/T}$	Monks *et al.* 1993
$C_3N + C_2H_2 \xrightarrow{279}$ soot + H	$8.6 \times 10^{-15} T^{1.8} e^{474/T}$	estimated, k($C_2H + C_2H_2$)
$C_3N + C_2H_4 \xrightarrow{280}$ soot + H	$7.8 \times 10^{-11} e^{134/T}$	estimated, k($C_2H + C_2H_4$)
$C_3N + C_4H_2 \xrightarrow{281}$ soot + H	$8.6 \times 10^{-16} T^{1.8} e^{474/T}$	estimated, k($C_2H + C_2H_2$)
$C_3N + HC_3N \xrightarrow{282}$ soot + H	$8.6 \times 10^{-16} T^{1.8} e^{474/T}$	estimated, k($C_2H + C_2H_2$)
$HC_3N + C_2H \xrightarrow{283}$ soot + H	$8.6 \times 10^{-16} T^{1.8} e^{474/T}$	estimated, k($C_2H + C_2H_2$)
$HC_3N + C_4H \xrightarrow{284}$ soot + H	$8.6 \times 10^{-16} T^{1.8} e^{474/T}$	estimated, k($C_2H + C_2H_2$)/3

The major parameters for this section are the strength of the winds, and the phase of the reversal with respect to the equinox. For the GCM results, which were obtained with opacity sources uniform in the horizontal plane and over the year, the reversal occurs around equinoxes. In a recent model, Tokano *et al.* (1999) obtained the same phase with uniformely distributed opacity sources, but they also ran their model under modified cooling rates, in order to take into account the seasonal variations of the radiatively active gases. This modification shifted the reversal by half a season, and also shortened the reversal period. In this paper, both cases are investigated: the ascending edge of the Hadley cells versus the solar longitude is indicated in Fig. 6.

Transport of chemical compounds by this prescribed mean meridional circulation is computed with a second-order finite volume scheme with slope limitation (Van Leer 1977, Hourdin and Armengaud 1999). We checked the possible impact of our poor latitudinal resolution (17 latitudes) by doubling the number of air columns from pole to pole (33 latitudes). Almost the same results were obtained as with the coarser grid.

Mixing by transient eddies. Horizontal eddy diffusion must be introduced to simulate transport by horizontal transient eddies which cannot be explicitly accounted for in a two-dimensional latitude–altitude model but that are present in the GCM results, especially near the 1-mbar level. These transient eddies

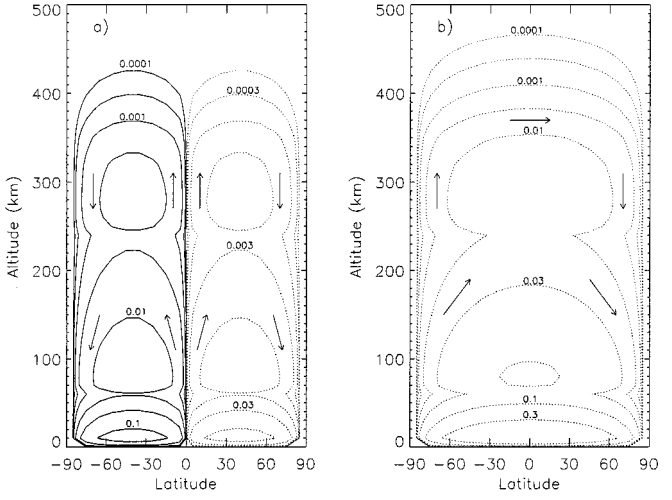

FIG. 4. Stream functions for the synthetic meridional winds, in 10^9 kg s^{-1} (solid line is direct rotation, dotted line is clockwise). (a) is the reversal (equinox or half a season later) and (b) is northern winter solstice.

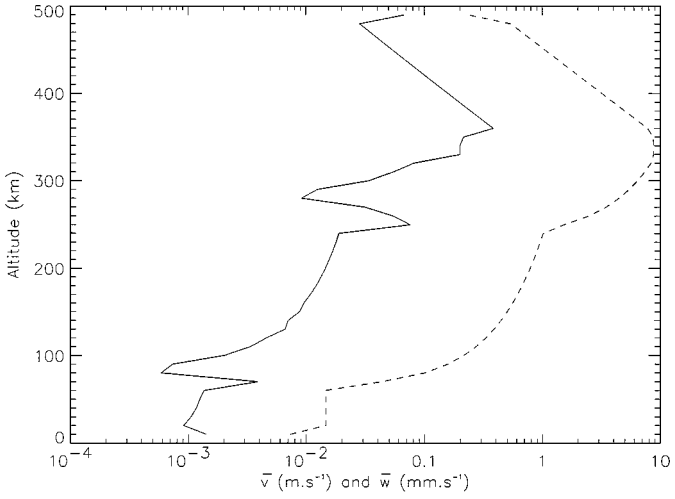

FIG. 5. Vertical profiles of the quadratic means of the reconstructed winds: meridional component $\bar{v}$ (solid line, in m s^{-1}) and vertical component $\bar{w}$ (dashed line, in mm s^{-1}).

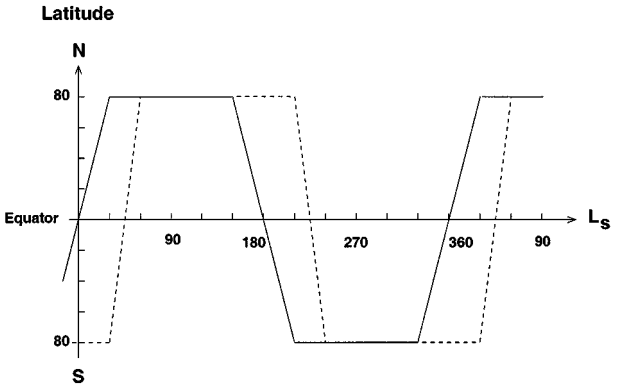

FIG. 6. Latitude of the ascending edge of the Hadley cells as function of the solar longitude. Solid line: the reversal occurs at equinox (Hourdin *et al.* 1995); dashed line: the reversal is faster and occurs half a season later (Tokano *et al.* 1999).

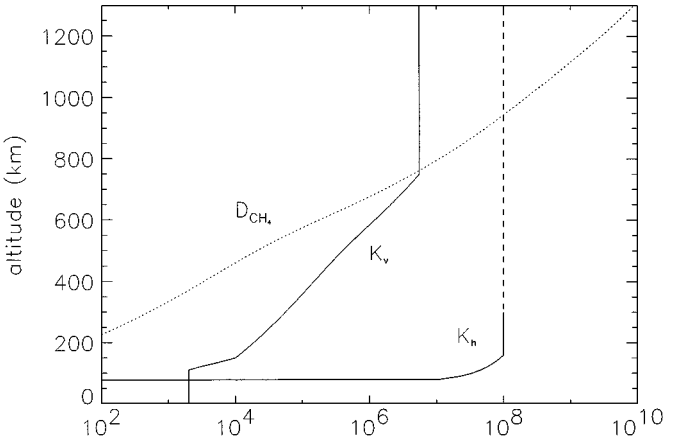

FIG. 7. Eddy diffusion coefficients: vertical (K_v) and horizontal (K_h) (solid lines), with the molecular diffusion coefficient (D_{CH_4}) of methane in nitrogen (dotted line) (units are $cm^2\ s^{-1}$).

transport angular momentum latitudinally, playing a central role in the maintenance of atmospheric superrotation (Hourdin *et al.* 1995). They also transport chemical species. In our model, the horizontal mixing by eddies was parameterized as an horizontal diffusion: for a given species i, we added to the continuity equation the term

$$\frac{\partial y_i(\phi, r)}{\partial t} = \frac{1}{r^2 \cos\phi} \frac{\partial}{\partial \phi} \left[\cos\phi K_h(\phi, r) \frac{\partial y_i(\phi, r)}{\partial \phi} \right],$$

where ϕ is the latitude, r the radial coordinate, y_i is the species' mole fraction, and n is the density. The diffusion coefficient K_h was crudely estimated from the GCM results (Hourdin *et al.* 1995, Fig. 13) as

$$K_h \sim \frac{|v'\mu'|R}{\mu},$$

where $|v'\mu'|$ represents the transient transport of angular momentum, μ is the angular momentum, and R is Titan's radius. The maximum wave activity is seen in the GCM in the stratosphere. The approximated vertical profile of this coefficient is shown in Fig. 7. Above 300 km, it is difficult to constrain this parameter, so it is assumed to be constant. No variations with latitude or time have been introduced.

We are currently working on a parameterization of this K_h coefficient based on studies with a dynamical horizontal (shallow-water) model. These studies will help us to constrain this coefficient as a function of altitude and also as a function of latitude, so that we can better represent transient horizontal eddies in two-dimensional (latitude–altitude) GCMs.

Vertical eddy diffusion. Below 500 km, the vertical eddy diffusion coefficient does not account for the same processes than in one-dimensional models, since advection is now explicit in the model. It is now restricted to representation of turbulent mixing, or dynamical phenomena that are not taken into account in the analytic description of the meridional circulation. This parameter (together with molecular diffusion) is the only description of dynamics above mesopause (~500 km), and it controls the exchanges between the regions below and above mesopause. As a first guess, the profile of this parameter was taken from Toublanc *et al.* (1995), and is shown in Fig. 7.

Dynamical timescales. For these three transport modes, timescales have been evaluated (Table VI). For vertical transport, the characteristic length is the scale height H and for horizontal transport we used the equator-pole distance $L \sim 4000$ km, leading to

$$\tau_v^K = \frac{H^2}{K_v} \quad \text{and} \quad \tau_h^K = \frac{L^2}{K_h}$$

for vertical and horizontal diffusion, respectively, and

$$\tau_v^W = \frac{H}{\bar{w}} \quad \text{and} \quad \tau_h^W = \frac{L}{\bar{v}}$$

for mean meridional transport, where $\bar{w}$ and $\bar{v}$ are the root mean

TABLE VI
Dynamical Timescales τ, in Unit $TY = 9.47 \times 10^8$ s (Titan Year)

	Horizontal dynamics	Vertical dynamics	Horizontal diffusion	Vertical diffusion	Altitude (km)
Turbopause	—	—	2.5	0.008	~800
High atmosphere	—	—	2.5	↕	
Mesopause	0.1	0.1	2.	0.04	~550
Mesophere	0.04	0.01	2.	↕	
Stratopause	0.1	0.01	2.	0.3	~250
Stratosphere	↕	↕	2.	↕	
Tropopause	4.	1.	10.	6.	~50
Troposphere	4.	1.	—	6.	

Note. These are approximate values. The arrows indicate an approximately linear variation of log τ with height.

squares of the vertical and meridional components of the wind speed for a given altitude at solstice (Fig. 5).

Numerical values are given in Table VI. These timescales give an idea of the dominant transport mechanism at different altitudes. Horizontal diffusion seems to be significant only in the low stratosphere. In the lower atmosphere where it has been introduced, the dynamical transport by winds appears to be the important mechanism, especially for vertical mixing with a strong influence on vertical profiles, as shown below.

Numerical aspects. Conservation of chemical elements is good in the model. Both the transport scheme (Hourdin and Armengaud 1999) and the continuity equations solver (Toublanc *et al.* 1995) have proven their accuracy. No effects of numerical diffusion could be detected: When horizontal or vertical dissipation are cut off, steep gradients appear in the composition profiles. Also, two different horizontal resolutions (17 and 35 latitudes) gave the same results.

3. RESULTS

3.1. High Atmosphere and Seasonal Oscillations

The high atmosphere ($z > 600$ km) is not well constrained by observations, except for CH_4 and C_2H_2 (Smith *et al.* 1982; Strobel *et al.* 1992; Vervack *et al.* 1999) and for the column density of HC_3N above 300 km (Bézard *et al.* 1992). In this region, where photolysis is the primary driver for chemistry, the composition undergoes a seasonal cycle, where the amplitude of the variations are related to the latitude (the higher the latitude, the larger the difference between summer and winter UV fluxes). This behavior is similar to the one described by Lebonnois and Toublanc (1999) (where no horizontal diffusion nor winds were included). In this case, these oscillations are located above 500 km. This altitude appears in the two-dimensional simulations as a node, a stable point for most species (Fig. 8). The influence of photochemical oscillations, propagated down by diffusion, decreases with altitude. On the other side, the oscillations resulting from dynamical transport are strongest in the stratosphere, and decrease when altitude increases. Since both oscillations are in opposite phase, this yields a stable region around 500 km of altitude, at the upper limit of the dynamical transport. However, this node may be partly model-dependent and this region, around mesopause, is still mostly unknown.

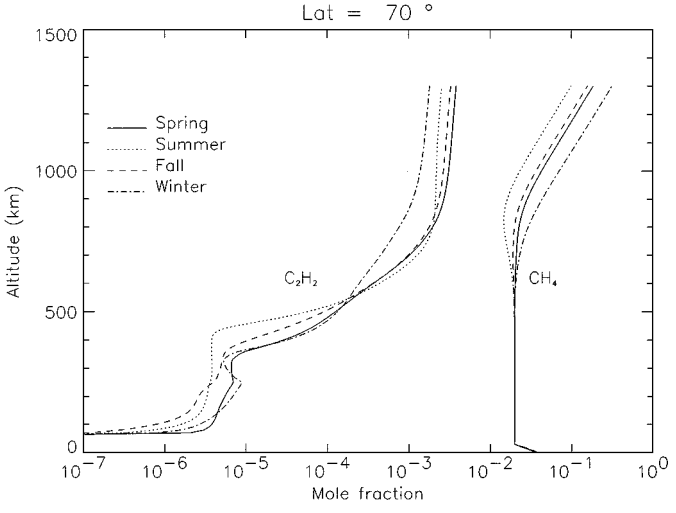

FIG. 8. Seasonal variations at 70°N for methane and acetylene. Most of the minor compounds are seasonally invariant around z = 500 km.

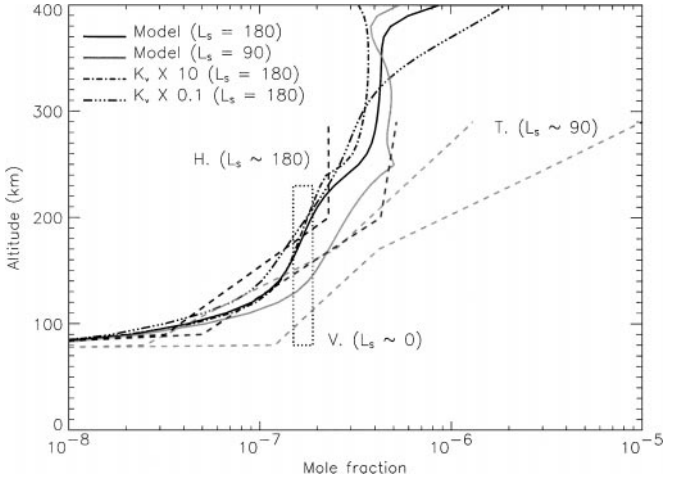

FIG. 9. Simulated profiles of HCN at equator. The reference simulation (black solid line for equinox, gray solid line for solstice) and the sensitivity tests with $K_v \times 10$ and $K_v \times 1/10$ (dashed–dotted lines, for equinox only) are compared to observations: ground-based millimeter observations from Tanguy *et al.* (1990) (gray dashed lines, delimiting the uncertainty domain) and from Hidayat *et al.* (1997) (black dashed lines), and VoyagerI/IRIS observations (Coustenis and Bézard 1995) (dotted box). The approximate solar longitude at Saturn is indicated for each observation.

3.2. Full Dynamics versus Eddy Mixing Approach

The use of eddy diffusion coefficient is generally considered in one-dimensional model as a way to represent vertical mixing by dynamics. But this ad-hoc coefficient hides a lot of physical processes, leading to a strong limitation in the use of one-dimensional models. Lara *et al.* (1996) performed a comparative study of different profiles of the vertical eddy coefficient for the atmosphere of Titan. In this study, it appears clearly that it is impossible to fit all the observed species with a unique vertical eddy coefficient, which is not a good point for a parameterization of transport. In particular, using the profile derived from the ground-based millimeter and submillimeter HCN observations by Hidayat *et al.* (1997) yields a mismatch for most of the hydrocarbons. It may be argued that some loss of N to the haze was not included in this study, which could affect HCN retrieval (McKay 1996; Lara *et al.* 1999). These possible problems in the chemical scheme make it difficult to determine the vertical eddy diffusion coefficient, which is another limit of this parameterization. We show in Fig. 9 the comparison of the HCN mole fraction (at equator) obtained from our two-dimensional photochemical model with the profiles retrieved from HCN observations (Tanguy *et al.* 1990, Hidayat *et al.* 1997). The modeled profile

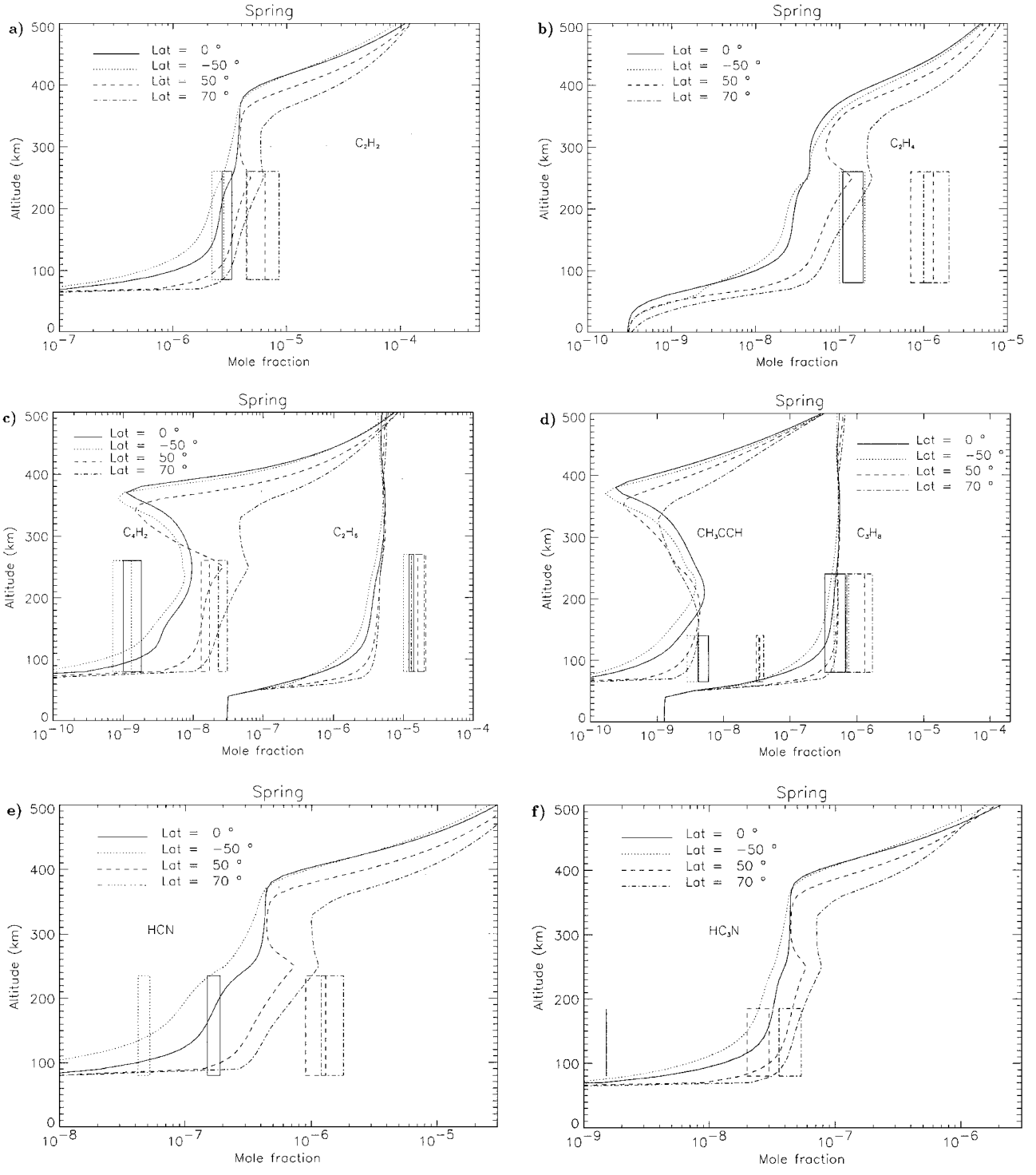

FIG. 10. Latitudinal variations at spring equinox for (a) C_2H_2, (b) C_2H_4, (c) C_2H_6 and C_4H_2, (d) CH_3C_2H and C_3H_8, (e) HCN, and (f) HC_3N. The boxes are from Voyager I observations, and their limits in height are given by the half-width of the contribution functions (Coustenis and Bézard, 1995).

is shown for the reference simulation (equinox and solstice), but also for the test runs (equinox only) with the vertical eddy coefficient scaled by factors of 0.1 and 10 (see Section 4). For both observations, the simulations are almost in the error bars. The difference between both retrievals is then clearly attributed to a seasonal effect. Note also the weak sensitivity to vertical diffusion. From this example, it clearly appears that the advantage of the two-dimensional approach is twofold: first, stratospheric levels at the equator are satisfactorily reproduced for most of the constituents (see Fig. 10) without any tuning. Second, these

results are much less sensitive to the choice of the vertical diffusion coefficient. This full description of the dynamics in the stratosphere allows a better representation not only of horizontal, but also of vertical mixing of chemical species.

3.3. Latitudinal Behavior in the Lower Atmosphere

We show in Fig. 10 the vertical profiles (below 500 km) of several species at the equator, 50° S, 50°, and 70° N at spring equinox, together with uncertainty boxes of Voyager observations. The limits in height for these boxes are the half-width of the contribution functions (Coustenis and Bézard 1995). The agreement is good for C_2H_2, C_3H_8, and HCN. For C_4H_2, we must notice that the relaxation rates of $C_4H_2^*$ (R212 + R213) are upper limits, and that the stratospheric level of C_4H_2 is sensitive to these values. When these rates are fixed to the upper-limit values, the C_4H_2 mole fraction at 100 km altitude is a factor of 10 above the observed level. We had to lower the relaxation rates by a factor of 5000 to reach agreement with the Voyager observations. This adjustment has no significant influence on other species. The stratospheric levels of C_2H_4, C_2H_6, and CH_3C_2H at the equator are slightly underestimated, and the mole fraction of HC_3N is overestimated. In the lower atmosphere ($z < 400$ km), the vertical profiles of most species are more homogeneous than in previous models, because of the large-scale motions introduced in this new model. The differences between the observed and modeled equatorial stratospheric compositions indicate that the photochemical scheme needs improvement in order to better understand this composition. The uncertainties on the chemical reaction rates can also be partly responsible for these problems. However, we will focus our discussion on the latitudinal variations of the mean composition, which are related to the vertical gradients of the species' profiles and to the two-dimensional transport, as shown below.

In Lebonnois and Toublanc (1999), we demonstrated that a model including the seasonal variations of the UV field, but without two-dimensional dynamics, could not induce the expected latitudinal variations in the stratospheric composition. With the introduction of the two-dimensional transport, the situation is much different. Figure 11 displays the latitudinal behavior of compounds as retrieved by Voyager observations and as obtained with this model (for altitudes corresponding to the maximum of the contribution functions, as indicated in the caption). From these results, and if we do not focus on the equatorial values, we can describe three different latitudinal behaviors at these altitudes: (1) species that undergo moderate latitudinal

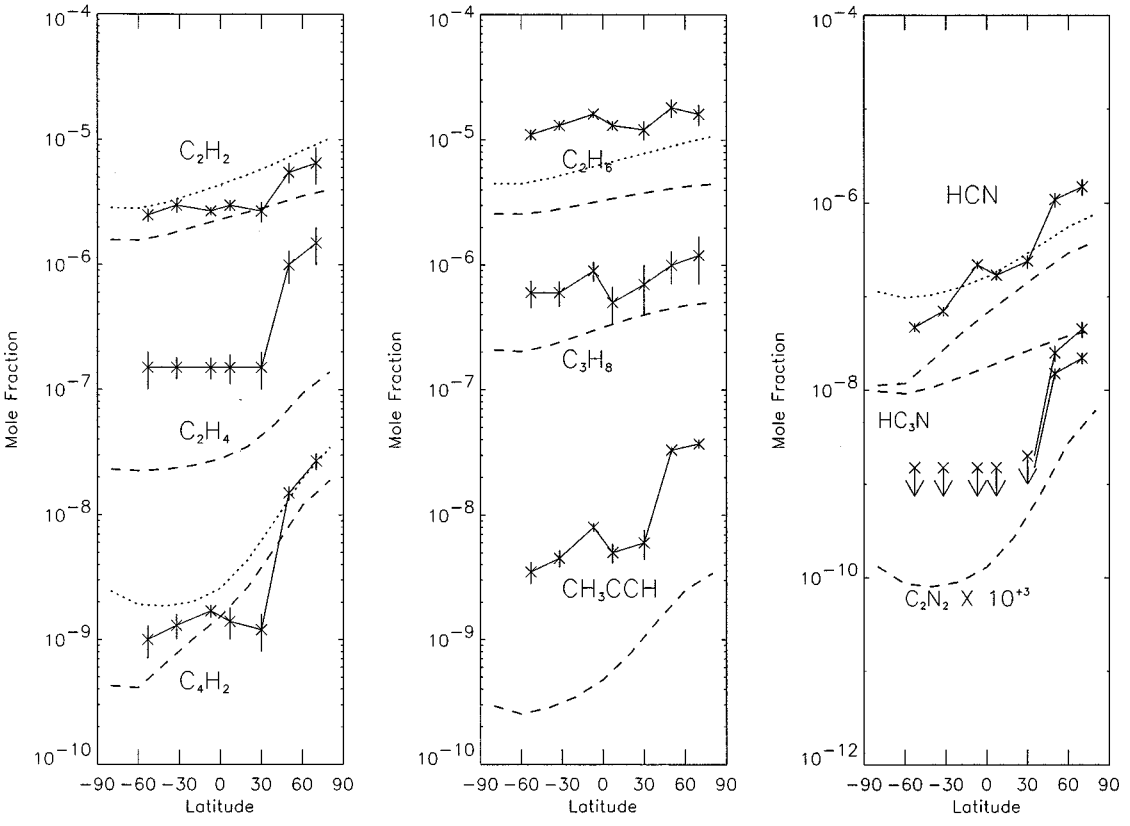

FIG. 11. Latitudinal variations of some components for the two-dimensional photochemical model (dashed lines), compared to the observed variations (solid lines). The altitude chosen is the approximate maximum of the contribution function: C_2H_2 (altitude = 150 km), C_2H_4 (180 km), C_4H_2 (100 km), C_2H_6 (160 km), C_3H_8 (125 km), CH_3C_2H (90 km), HCN (105 km), HC_3N (105 km), C_2N_2 (80 km). The dotted lines correspond to idealized tracers (see text).

variations that are reproduced by the model (C_2H_2, C_2H_6, C_3H_8), (2) species that undergo important latitudinal variations that are more or less reproduced by the model (C_2H_4, CH_3C_2H, C_4H_2, and HCN), (3) species that undergo important latitudinal variations that are underestimated by the model (HC_3N). We must notice that in this model, the horizontal eddy coefficient is considered uniform in latitude, which is a poor approximation of real dissipative motions (Luz and Hourdin 1999). In Fig. 12, we show the two-dimensional distribution of C_2H_2 and HCN at northern spring equinox and at the following solstice. These distributions clearly suggest that the latitudinal contrasts we observe in the low stratosphere are the result of the large-scale transport that has now been included in the model. Between both seasons, after the reversal of the Hadley circulation, the descending (ascending) motions at the southern (northern) pole seem to reverse the stratospheric contrasts, which keep increasing until the next reversal.

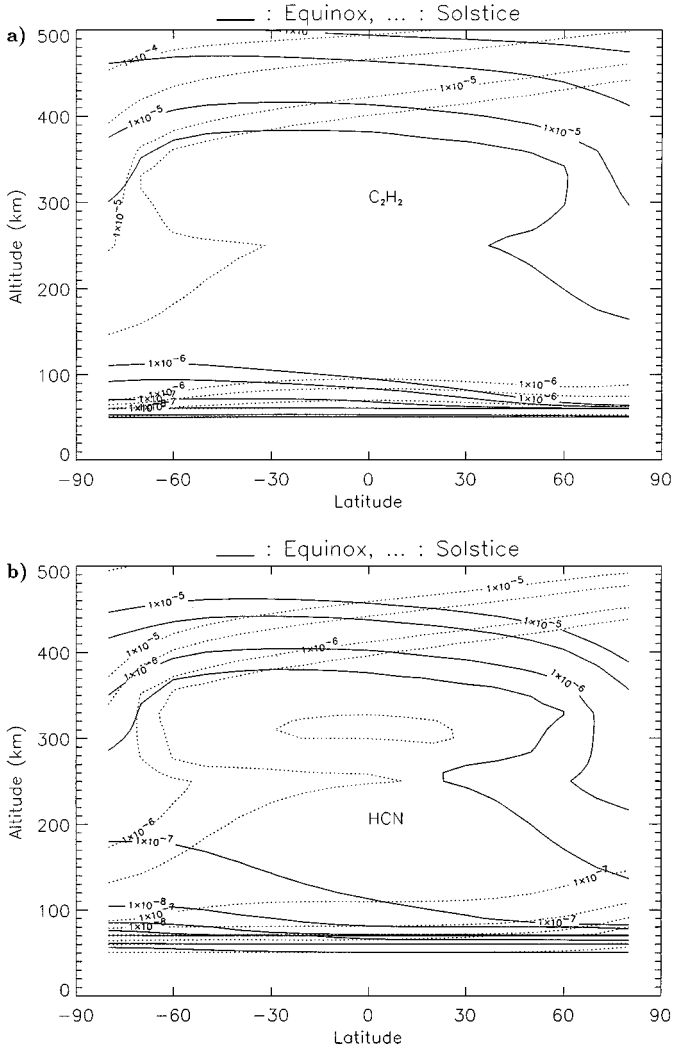

FIG. 12. Altitude–latitude mole fractions of (a) C_2H_2 and (b) HCN, at northern spring equinox (solid lines), and at the following solstice (i.e., northern summer solstice, dotted lines).

3.4. Idealized Tracers

Thus, the results above suggest that the latitudinal structure in the low stratosphere results from vertical transport in an atmosphere where concentrations of chemical species increase vertically. To confirm this hypothesis, we have done two other types of simulations. First, we have run a two-year simulation similar to the reference run, except that the UV field was constant in time and latitude, equal to the spring equatorial situation. Small differences in the resulting composition were obtained below 500 km, but the seasonal and latitudinal behavior of each compound was very close to the reference simulation. Second, we applied the same two-dimensional atmospheric transport to idealized tracers for which the full chemistry is replaced by a simple linear relaxation toward a prescribed vertical profile, independent of time and latitude. This approach reduces enormously the computer time, but can still describe the situation fairly well, as will be shown below. For a given species i, we use as relaxation profile $y_i^o(z)$ the equilibrium profile of a one-dimensional photochemical simulation. The relaxation time constant $\tau_i(z)$ is taken as the time and latitudinal average of the chemical timescale

$$\tau_i(z,\phi,t) = \left| \frac{y_i^o(z) - y_i(z,\phi,t)}{\sum_R \left(\frac{\partial y_i}{\partial t}\right)(z,\phi,t)} \right|$$

derived from the two-dimensional simulations, where $y_i(z, \phi, t)$ is the mole fraction of species i at the given altitude z, latitude ϕ, and time t, and the sum is done over all the chemical reactions involving the species i. For idealized tracers, the model uses the same grid (limited to 500 km in altitude) and the same dynamical transport by winds and horizontal eddies than the photochemical model. Vertical eddy diffusion is also included and condensation in the troposphere is taken into account. From the reference vertical profile (uniform in latitude), the tracer is transported for two Titan years, which yields satisfying steady oscillations.

The cases of C_2H_2, C_2H_6, C_4H_2, and HCN were investigated with this idealized tracer approach. Relaxation profiles $y_i^0(z)$ and time constants $\tau_i(z)$ are given in Fig. 13. The relaxation profiles increase with altitude, and this induces stratospheric latitudinal contrasts. The results are very close to those obtained with the full chemistry (Fig. 11). The global distributions are also approximately reproduced by this simple approach (Fig. 14, to be compared to Fig. 12). This shows that latitudinal contrasts can be explained without any seasonal variation of the UV field nor any complex nonlinearity of the chemistry. The latitudinal contrasts are just the result of an increase of the mole fractions at latitudes where there is a downwelling motion, because species are more abundant higher in the atmosphere. Figure 15 illustrates this dominant mechanism. For example, the strong contrast obtained for the C_4H_2 tracer is essentially due to the large difference between the mole fraction at $z = 100$ km ($\sim 10^{-9}$ at the equator) and at $z = 500$ km ($\sim 10^{-6}$–10^{-5}). Of course, deposition of UV radiation and chemistry play an important role in the formation of latitudinal contrasts in the low stratosphere,

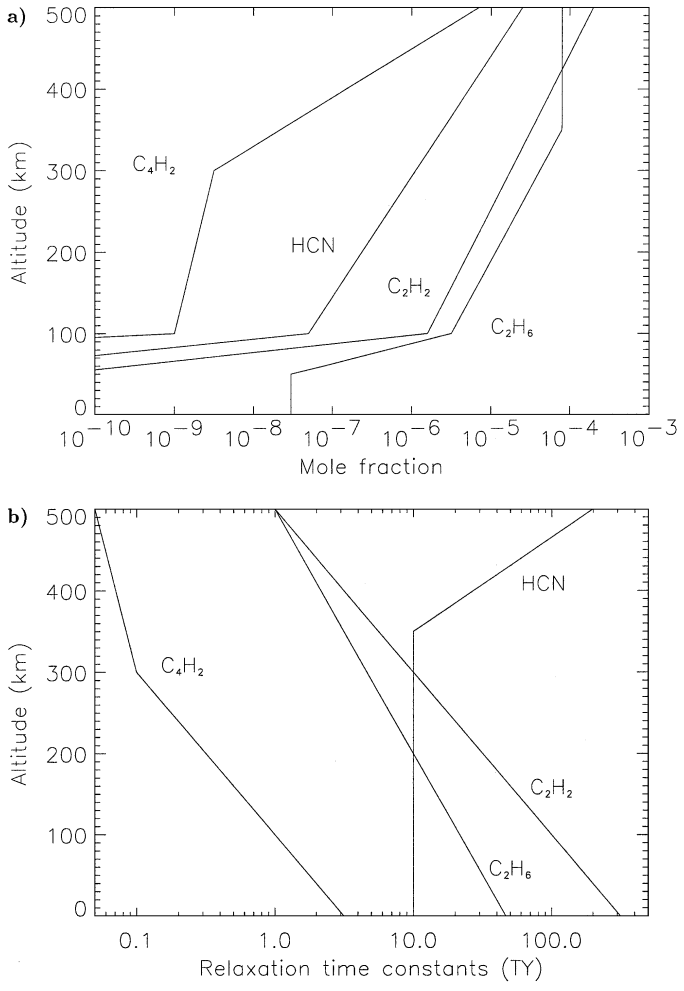

FIG. 13. (a) Relaxation profiles of mole fractions y_i^o and (b) relaxation time constants τ_i (in unit $TY = 9.47 \times 10^8$ s) used in the idealized tracers' approach for some chemical species.

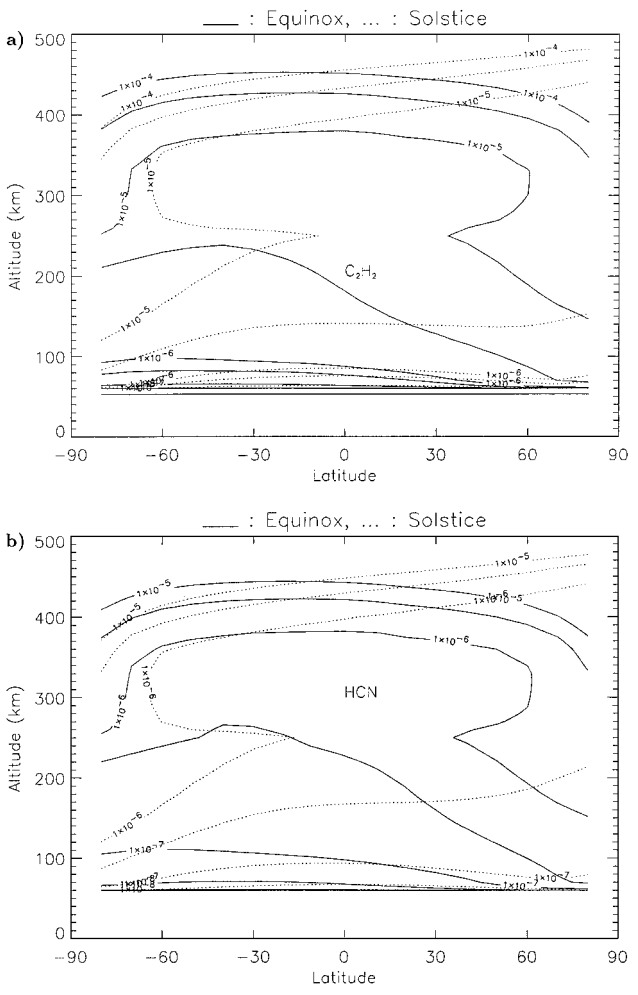

FIG. 14. Same as Fig. 12, but for the idealized tracers corresponding to (a) C_2H_2 and (b) HCN.

but only by modifying the mean equilibrium vertical gradient of the chemical species.

We can conclude that the observed latitudinal profiles in the low stratosphere are indicators of the dynamical structure of the lower atmosphere, which gives the shape, and of the chemical schemes, which act on the amplitude of the contrasts through the vertical distribution of the species and their chemical timescales. The mismatch between the modeled behavior of HC_3N and its observed stratospheric latitudinal profile strongly suggests that the problem comes from the chemical scheme in the lower atmosphere.

4. SENSITIVITY TO DYNAMICAL PARAMETERS

The results appear to be satisfying with the a priori values of the different dynamical parameters used in the reference simulation. However, since the model is complex, it is important

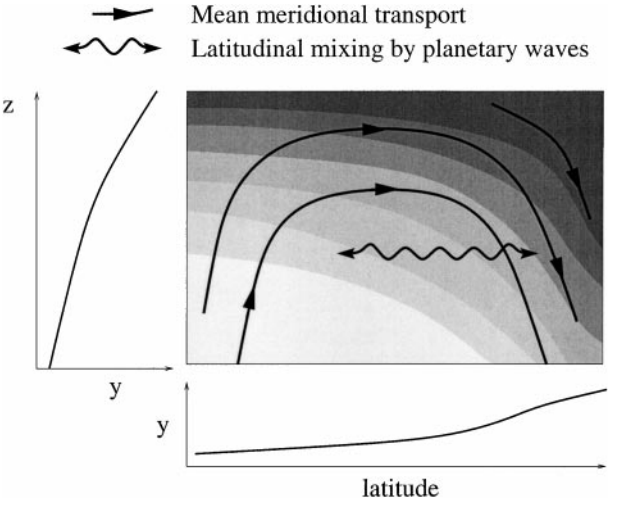

FIG. 15. Impact of dynamics on the distribution of chemical compounds. This impact appears to be the dominant effect on latitudinal contrasts.

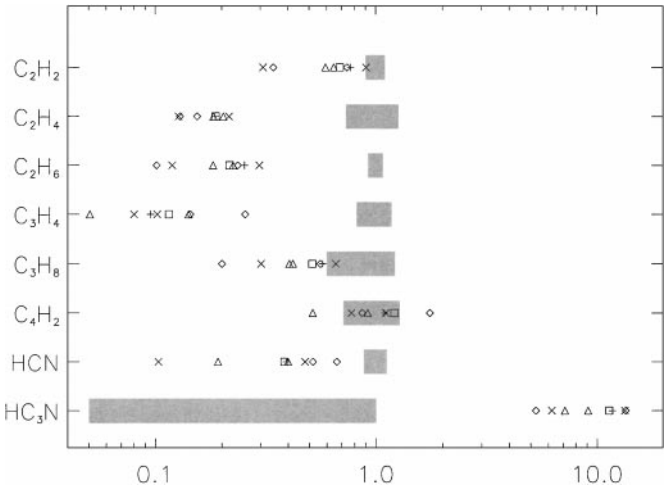

FIG. 16. Sensitivity tests: Equatorial mixing ratios, normalized to the recommended values from Coustenis and Bézard (1995). The uncertainty limits for these observations are shown as light gray boxes. The results of the test runs of the 2-D photochemical model (at the corresponding altitudes) are plotted with symbols: diamonds for $K_v \times 10$ and $K_v \times 1/10$, triangles for $K_h \times 10$ and $K_h \times 1/10$, crosses ($\times$) for wind speed $\times 1/2$ and wind speed $\times 2$, squares for the shifted reversal test and plus signs for the reference simulation.

to have an idea of the impact of each parameter. For this, we made several limited runs (some of which have already been mentioned), changing each time one parameter: (1) the vertical eddy coefficient was scaled by factors of 10 and 1/10, (2) the horizontal eddy coefficient was scaled by factors of 10 and 1/10, (3) the strength of the winds was scaled by factors of 1/2 and 2. We also ran the model with a different phase for the seasonal reversal of the winds. Since this model has a heavy numerical cost, these runs were limited by two aspects: though the reference simulation was done for four Titan years in order to achieve a good steady-state cycle, the sensitivity simulations were limited to one Titan year, except for the phase of the reversal (two TY). Though this is not long enough, the differences between two symmetrical seasons were small. As seen in Table VI, most timescales above 100 km are less (or around) one Titan year, except for horizontal dissipation. When K_h is stronger, the timescale is less and the effects are clear even after only one Titan year (the stratosphere is more uniform), and when this coefficient is lower, the dominant horizontal mixing is due to transport.

So we can expect that these tests give a good idea of the first-order sensitivity, especially for the latitudinal contrasts. The height of the atmosphere was also limited to 500 km (taking advantage of the node we see in the composition), except for tests on the vertical eddy coefficient. We ran a simulation with these limitations and the reference values of the parameters: except above 400 km where some differences were visible because of the limited height of the atmosphere, the test was almost identical to the reference results in the stratosphere. We display in Fig. 16 and 17 the main effects of these tests on two sets of data comparable to the Voyager I observations (therefore concerning

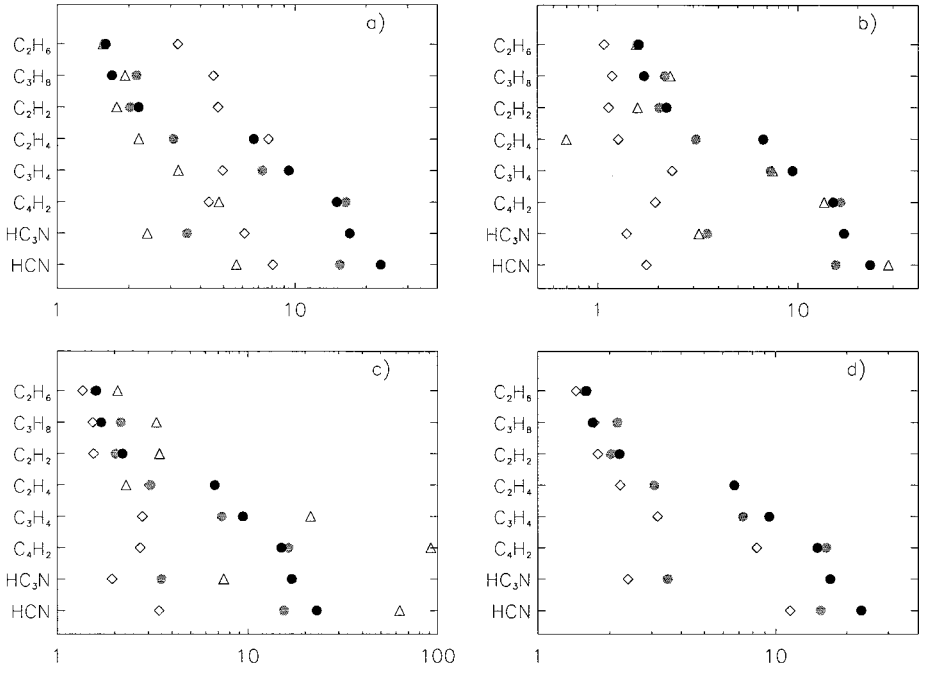

FIG. 17. Sensitivity tests: Ratio between the 50°N mole fractions and the 50°S ones. The results from Coustenis and Bézard (1995) are shown as black circles, the reference simulation of the 2-D photochemical model (at the corresponding altitudes) as gray circles, and the results of the tests runs are shown as: (a) diamonds for $K_v \times 10$ and triangles for $K_v \times 1/10$, (b) diamonds for $K_h \times 10$, and triangles for $K_h \times 1/10$, and (c) diamonds for wind speed $\times$ $1/2$ and triangles for wind speed $\times 2$. (d) diamonds for shifted reversal test.

the low stratosphere: 80–150 km): the equatorial mole fractions, and the ratio between mole fractions at 50° N and 50° S to explore the enrichment of high latitudes and the asymmetry of this enrichment. Generally, changing the dynamics strongly affects latitudinal contrasts. The equatorial values seem to be essentially controlled by chemistry, though some species are affected by variations of dynamical parameters (Fig. 16).

For the tests on the vertical eddy coefficient, the essential effects are seen in the high atmosphere ($z > 500$ km), where the mean meridional circulation is not explicitly accounted for. This parameter has an influence on the stratosphere through the exchange that takes place around 500 km. It affects the composition in the mid-atmosphere, and therefore can influence latitudinal contrasts. This effect is more visible for C_2H_2, C_2H_4, C_2H_6, C_3H_8, and HC_3N, species that are sensitive to transport through the mesopause. The influence of the vertical eddy coefficient on the high-atmosphere levels is also interesting. In a recent reanalysis of the Voyager I/UVS solar occultation data, Vervack *et al.* (1999) concluded that the structure of the high atmosphere is different than previously derived by Smith *et al.* (1982). In particular, methane mixing ratio is still around 2% above 1000 km, and the mixing ratio of C_2H_2 they retrieve is approximately a hundred times less than the previous results. This reanalysis will have to be taken into account for future models of the high atmosphere of Titan. The test with stronger eddy coefficient shows a C_2H_2 mixing ratio in the high atmosphere that was similar to the one derived by Vervack *et al.* The high-atmosphere mole fractions are very sensitive to the vertical eddy coefficient, suggesting that this parameter could be adapted in order to fit the new results. The wind strength and the horizontal eddy coefficient K_h have a strong effect on the latitudinal behavior of the stratospheric composition, as shown in Fig 17. Slower winds or stronger K_h have roughly the same effect: the lower atmosphere is more uniform in latitude. On the other hand, stronger winds enhance the contrast, as well as lower values of K_h (as this parameter decreases, contrast is controlled by the wind strength).

The profiles that fit the best with the observations in these test runs are obtained for the ($K_h \times 0.1$) test. Note that for this test, the ethylene profile exhibits a small increase toward the south pole, while the strong enhancement in the north begins after 50° N, which explains the only point lower than 1 (Fig. 17). From the composition obtained with the phase shift, we can deduce that the influence of the exact moment of the reversal is not strong: the latitudinal profiles at the equinox are fairly similar in both cases. This can be explained because the latitudinal contrasts are built during the period after the solstice, and stay visible until the reversal. Whether this reversal happens just at the equinox or half a season later only slightly affects the contrasts at the time of Voyager encounter.

5. CONCLUSION

Introduction of two-dimensional transport in a rather sophisticated photochemical model yields, for the first time, to a satisfactory and self-consistent simulation of the latitudinal profiles of the concentration of chemical species retrieved by Voyager 1 for the low stratosphere. These latitudinal contrasts are reproduced as well by a much simpler model with the same meridional circulation and latitudinal mixing by eddies (both deduced from numerical simulations of the atmospheric circulation) and chemical species relaxed toward a fixed vertically increasing profile.

Thus, at least in our model, the latitudinal contrasts are unambiguously attributed to meridional transport: downward transport from the enriched upper atmosphere leads in a local enrichment below. In this self-consistent explanation, latitudinal and seasonal variations of the UV field play no role. Photochemistry essentially controls the planetary mean vertical profiles and time constants. In turn, both the mean vertical gradient and time constant of course have an impact on the latitudinal contrasts.

This has two important consequences. First, an accurate prescription of the 2-D distribution of the UV field is probably of secondary importance for determining latitudinal contrasts in the low stratosphere. This indeed confirms the previous study by Lebonnois and Toublanc (1999). Thus, the potential effect of seasonal variations of the haze distribution (very difficult to guess with the current status of observation or modeling) is also of secondary importance for our purpose. Second, if we believe that the chemistry model gives a good description of vertical profiles (as suggested by comparisons with the available observations), the good agreement with Voyager data, in terms of latitudinal contrasts, gives a unique constraint on the vertical winds in the lower stratosphere and an interesting a posteriori validation of the simulations by Hourdin *et al.* (1995). However, our sensitivity experiments show that the comparison with Voyager data does not completely constrain the phase of the reversal of the mean meridional circulation. A reversal at equinoxe or some time later would be compatible with Voyager observations since the building of these latitudinal contrasts occurs between reversal and solstice.

There are certainly problems in the chemical schemes for C_2H_4, HC_3N, and C_2N_2 since their equatorial values in the low stratosphere do not match the observations (neither do HC_3N latitudinal contrasts). For all species but for HC_3N, latitudinal, contrasts are satisfactorily reproduced. Note also that differences between Tanguy *et al.* (1990) and Hidayat *et al.* (1997) observations are compatible with our results and interpreted as a seasonal effect. The mismatch in the details of the shape of the modeled latitudinal profiles with the shape of the observed profiles can be explained by the simple parameterization used for the meridional wind field and for the horizontal eddy coefficient. The understanding of the latitudinal distributions observed by Voyager is tied to a better understanding of the dynamics of the stratosphere and mesosphere, and its interactions with the different components of the atmosphere: the haze layer and the trace species distributions.

Some of these trace species have an influence on the cooling rates in Titan's stratosphere and their latitudinal variations

may have an impact on latitudinal temperature contrasts, as shown by Bézard *et al.* (1995). To go further in the comprehensive modeling of the lower part of the atmosphere of Titan, we are now developing a coupled GCM-photochemistry two-dimensional model. This model should be an important tool to analyze and understand the abundant and detailed observations that the Cassini–Huygens mission will make of Titan's atmosphere.

APPENDIX: WINDS RECONSTRUCTION

The reconstruction of the meridional winds was based on the mean value of the vertical component of the wind speed w_0, as a function of altitude, obtained from the GCM. Below 60 km, $w_0(z)$ is constant and equal to $1. \times 10^{-5}$ m s^{-1} (except at the surface: $w_0(z=0)=0$); it linearly increases to $7. \times 10^{-4}$ m s^{-1} at $z = 240$ km, and then to $6. \times 10^{-3}$ m s^{-1} at $z = 320$ km. The GCM did not go higher than 300 km, so we extrapolated $w_0(z)$ upward by decreasing it exponentially down to zero at 500 km. To reconstruct the latitudinal and seasonal variations of the vertical wind speed, we built a time-dependent latitudinal factor $f(\phi, L_S)$, where ϕ is the latitude and L_S is the solar longitude $-f$ is a sine function going from 1 at the ascending pole to -1 at the subsiding one when the Hadley cell is pole-to-pole. During the reversal, $f(\phi, L_S)$ is composed of two sinusoids, with maximum following the ascending latitude ϕ_A. The general shape for $f(\phi, L_S)$ is

$$\phi > \phi_A \ : \ f(\phi, L_S) = \cos\left[\pi \frac{\phi - \phi_A}{\phi_A - \phi_N}\right]$$

$$\phi < \phi_A \ : \ f(\phi, L_S) = \cos\left[\pi \frac{\phi_A - \phi}{\phi_A + \phi_N}\right],$$

where $\phi_N = 80^\circ$ is the latitude of the north pole grid point. When $\phi_A \neq \pm\phi_N$, $f(\phi_A)$ is doubled in order to satisfy mass conservation. According to what was obtained in the GCM, this factor is also decreased during the reversal so that it reaches a minimum when the ascending latitude is at the equator (one third of the solstice value). The two-dimensional vertical component of the mass flux $w_m(\phi, z, L_S)$ (in kg s^{-1}) can then be calculated as

$$w_m(\phi, z, L_S) = f(\phi, L_S) w_0(z) \frac{m_0(z)}{\Delta z},$$

where $m_0(z)$ is the mean mass of a two-dimensional grid cell, and $\Delta z = 10$ km is the vertical step. The meridional component of the mass flux $v_m(\phi, z, L_S)$ is computed from mass conservation (the divergence of the mass flux is equal to zero for each cell). This reconstruction yields the Hadley cells that are shown in Fig. 4, which can be compared to the GCM results (Fig. 6 in Hourdin *et al.* 1995). The shape of the extrapolation from the maximum value of $w_0(z)$ ($w_0(320\text{ km}) = 6 \times 10^{-3}$ m s^{-1}) down to zero at 500 km has no real influence on the mesospheric Hadley cell, since its center is located below 300 km. From $w_m(\phi, z)$ (resp. $v_m(\phi, z)$) at solstice, we computed $\bar{w}(z)$ (resp. $\bar{v}(z)$) as

$$\bar{w}(z) = \left[\frac{1}{N_\phi} \sum_\phi \left(w_m(\phi, z) \frac{\Delta z}{m(\phi, z)}\right)^2\right]^{1/2},$$

$$\bar{v}(z) = \left[\frac{1}{N_\phi} \sum_\phi \left(v_m(\phi, z) \frac{\Delta L(z)}{m(\phi, z)}\right)^2\right]^{1/2},$$

where $m(\phi, z)$ is the mass of the grid cell at altitude z and latitude ϕ, $N_\phi = 17$ is the number of latitudes in the model, and $\Delta L(z)$ is the meridional length of a grid cell. The profiles of $\bar{w}(z)$ (mm s^{-1}) and $\bar{v}(z)$ (m s^{-1}) are presented in Fig. 5.

ACKNOWLEDGMENT

This work was supported by the Programme National de Planétologie of the Institut National des Sciences de l'Univers (CNRS).

REFERENCES

Aleksandrov, E. N., V. I. Vedeneev, S. N. Kozlov, A. A. Obvivalneva, and G. A. Pryakhin 1990. Rate constants and mechanism of the reactions of N(^{4}S) atoms with methane and ethane. *Bull. Acad. Sci. URSS, Div. Chem. Sci.* **39**, 625.

Arthur, N. L. 1986. Methyl radical absorption cross section at 216.4 nm and rate constant for methyl radical recombination. *J. Chem. Soc. Faraday Trans. 2* **82**, 331–336.

Atakan, B., and J. Wolfrum 1992. Kinetic studies of the reactions of CN radicals with alkanes in the temperature range between 294 and 1260 K. *Chem. Phys. Lett.* **186**, 547–552.

Back, R. A., and D. W. L. Griffiths 1967. Flash photolysis of ethylene. *J. Chem. Phys.* **46**, 4839–4843.

Baulch, D. L., C. J. Cobbs, R. A. Cox, C. Esser, P. Frank, Th. Just, J. A. Kerr, M. J. Pilling, J. Troe, R. W. Walker, and J. Warnatz 1992. Evaluated kinetic data for combustion modeling. *J. Phys. Chem. Ref. Data* **21**, 411–734.

Baulch, D. L., C. J. Cobbs, R. A. Cox, C. Esser, P. Frank, Th. Just, J. A. Kerr, M. J. Pilling, J. Troe, R. W. Walker, and J. Warnatz 1994. Evaluated kinetic data for combustion modeling. Supplement I. *J. Phys. Chem. Ref. Data* **23**, 847.

Bénilan, Y., P. Bruston, F. Raulin, C. Cossart-Magos, and J.-C. Guillemin 1994. Mid-UV spectroscopy of propynenitrile at low temperature: Consequences on expected results from observations of Titan's atmosphere. *J. Geophys. Res.* **99**, 17069–17074.

Bézard, B., A. Marten, and G. Paubert 1992. First ground-based detection of cyanoacetylene on Titan. *Bull. Am. Astron. Soc.* **24**, 953.

Bézard, B., A. Marten, and G. Paubert 1993. Detection of acetonitrile on Titan. *Bull. Am. Astron. Soc.* **25**, 1100.

Bézard, B., A. Coustenis, and C. P. McKay 1995. Titan's stratospheric temperature asymmetry: A radiative origin? *Icarus* **113**, 267–276.

Böhland, T., F. Temps, and H. Gg. Wagner 1985a. The contributions of intersystem crossing and reaction in the removal of $CH_2(\tilde{a}\,^1A_1)$ by hydrocarbons studied with the LMR. *Ber. Bunsenges. Phys. Chem.* **89**, 1013–1018.

Böhland, T., F. Temps, and H. Gg. Wagner 1985b. Kinetics of the reactions between $CH_2(X^3B_1)$ radicals and saturated hydrocarbons in the temperature range 296–707 K. *Ber. Bunsenges. Phys. Chem.* **89**, 1110.

Böhland, T., F. Temps, and H. Gg. Wagner 1988. Kinetics of the reactions between $CH_2(X^3B_1)$ radicals and saturated hydrocarbons in the temperature range 296–707 K. In *21st International Symposium on Combustion*, p. 841. The Combustion Institute, Pittsburgh.

Braun, W., J. R. McNesby, and A. N. Bass 1967. Flash photolysis of methane in the vacuum ultraviolet. II. Absolute rate constants for reactions of CH with methane, hydrogen and nitrogen. *J. Chem. Phys.* **46**, 2071.

Brown, R. L. 1973. Measurement of the rate of the reaction N + H + M = NH + M. *Int. J. Chem. Kinet.* **5**, 663.

Brownsword, R. A., S. D. Gatenby, L. B. Herbert, I. W. M. Smith, D. W. A. Stewart, and A. C. Symonds 1996. Kinetics of reactions between neutral free radicals. Rate constants for the reaction of CH radicals with N atoms between 216 and 584 K. *J. Chem. Soc. Faraday Trans.* **92**, 723–727.

Brownsword, R. A., A. Canosa, B. R. Rowe, I. R. Sims, I. W. M. Smith, D. W. A. Stewart, A. C. Symonds, and D. Travers 1997. Kinetics over a wide range of temperature (13-744 K): rate constants for the reaction of CH(v = 0) with H_2 and D_2 and for the removal of CH(v = 1) by H_2 and D_2. *J. Chem. Phys.* **106**, 7662–7677.

Butler, J. E., J. W. Fleming, L. P. Goss, and M. C. Lin 1981. Kinetics of CH radical reactions with selected molecules at room temperature. *Chem. Phys.* **56**, 355.

Calvert, J. G., and J. N. Pitts 1966. *Photochemistry.* Wiley, New York.

Campbell, I. M., and B. A. Thrush 1967. The recombination of nitrogen atoms and the nitrogen afterglow. *Proc. R. Soc. London* **296**, 201–221.

Canosa, A., I. R. Sims, D. Travers, I. W. M. Smith, and B. Rowe 1997. Reactions of the methylidine radical with CH_4, C_2H_2, C_2H_4, C_2H_6, and but-1-ene studied between 23 and 295 K with a CRESU apparatus. *Astron. Astrophys.* **323**, 644–651.

Clarke, D. W., and J. P. Ferris 1995. Photodissociation of cyanoacetylene: Application to the atmospheric chemistry of Titan. *Icarus* **115**, 119–125.

Collin, G. J., H. Deslauriers, and J. Deschênes 1979. Photolyse du propène et du méthyl-2-butène-2 vers 174 et à 163 nm. *Can. J. Chem.* **57**, 870–875.

Connors, R. E., J. L. Roebber, and K. Weiss 1974. Vacuum ultraviolet spectroscopy of cyanogen and cyanoacetylenes. *J. Chem. Phys.* **60**, 5011–5024.

Cooper, G., G. R. Burton, and C. E. Brion 1995a. Absolute UV and soft X-ray photoabsorption of acetylene by high resolution dipole (e,e) spectroscopy. *J. Electron Spectrosc. Rel. Phenomena* **73**, 139–148.

Cooper, G., T. N. Olney, and C. E. Brion 1995b. Absolute UV and soft X-ray photoabsorption of ethylene by high resolution dipole (e,e) spectroscopy. *Chem. Phys.* **194**, 175–184.

Coustenis, A., and B. Bézard 1995. Titan's atmosphere from Voyager infrared observations.IV. Latitudinal variations of temperature and composition. *Icarus* **115**, 126–140.

Dobrijevic, M., and J. P. Parisot 1998. Effects of chemical kinetics uncertainties on hydrocarbon production in the stratosphere of Neptune. *Planet. Space Sci.* **46**, 491–505.

Doepker, R. D. 1968. Vacuum-ultraviolet photolysis of the C_4H_6 isomers. I. 1,3-Butadiene. *J. Phys. Chem.* **72**, 4037–4042.

Du, H., J. P. Hessler, and P. J. Ogren 1996. Recombination of methyl radicals. I. New data between 1175 and 1750 K in the falloff region. *J. Phys. Chem.* **100**, 974–983.

Duràn, R. P., V. T. Amorebieta, and A. J. Colussi 1988. Is the homogeneous thermal dimerization of acetylene a free-radical chain reaction? Kinetic and thermochemical analysis. *J. Phys. Chem.* **92**, 636–640.

Fahr, A., and A. K. Nayak 1994. Temperature dependent ultraviolet absorption cross sections of 1,3-butadiene and butadiyne. *Chem. Phys.* **189**, 725–731.

Fahr, A., and A. K. Nayak 1996. Temperature dependent ultraviolet absorption cross sections of propylene, methylacetylene and vinylacetylene. *Chem. Phys.* **203**, 351–358.

Fahr, A., and S. E. Stein 1989. Reactions of vinyl and phenyl radicals with ethyne, ethene, and benzene. In *22nd International Symposium on Combustion*, p. 1023. The Combustion Institute, Pittsburgh.

Fahr, A., A. Laufer, R. Klein, and W. Braun 1991. Reaction rate determinations of vinyl radical reactions with vinyl, methyl, and hydrogen atoms. *J. Phys. Chem.* **95**, 3218–3224.

Fennelly, J. A., and D. G. Torr 1992. Photoionization and photoabsorption cross sections of O, N_2, O_2, and N for aeronomic calculations. *At. Data Nucl. Data Tables* **51**, 321–363.

Ferris, J. P., and J. C. Guillemin 1990. Photochemical cycloaddition reactions of cyanoacetylene and dicyanoacetylene. *J. Org. Chem.* **55**, 5601–5606.

Flasar, F. M., and B. J. Conrath 1990. Titan's stratospheric temperatures: A case for dynamical inertia? *Icarus* **85**, 346–354.

Forst, W. 1991. Microcanonical variational theory of radical recombination by inversion of interpolated partition function, with examples: $CH_3 + H$, $CH_3 + CH_3$. *J. Phys. Chem.* **95**, 3612–3620.

Fuke, K., and O. Schnepp 1979. Absorption and magnetic dichroism spectra of allene. *Chem. Phys.* **38**, 211–216.

Fulle, D., and H. Hippler 1997. The temperature and pressure dependence of the reactions $CH + H_2 \leftrightharpoons CH_3 \leftrightharpoons CH_2 + H$. *J. Chem. Phys.* **106**, 8691–8698.

Galand, M., J. Lilensten, D. Toublanc, and S. Maurice 1999. The ionosphere of Titan: Ideal diurnal and nocturnal cases. *Icarus* **140**, 92–105.

Gierczak, T., J. Gawlowski, and J. Niedzielski 1988. Reactions of excited C_3H_5 radicals: Implications for the photolysis of propylene at 8.4 eV. *J. Photochem. Photobiol. A.* **43**, 1–9.

Gladstone, G. R., M. Allen, and Y. L. Yung 1996. Hydrocarbon photochemistry in the upper atmosphere of Jupiter. *Icarus* **119**, 1–52.

Glicker, S., and H. Okabe 1987. Photochemistry of diacetylene. *J. Phys. Chem.* **91**, 437–440.

Haider, N., and D. Husain 1992. Kinetic investigation of the reactions of ground-state atomic carbon, C[2p2(3PJ)], with acetylenes by time-resolved atomic resonance absorption spectroscopy in the vacuum ultraviolet. *Z. Chem. Phys. (Munich)* **176**, 133–150.

Haider, N., and D. Husain 1993. Absolute rate data for the reactions of ground-state atomic carbon, C[2p2(3PJ)], with alkenes investigated by time-resolved atomic resonance absorption spectroscopy in the vacuum ultraviolet. *J. Chem. Soc. Faraday Trans.* **89**, 7–14.

Halberstadt, M. L., and J. Crump 1973. Insertion of methylene into the carbon-hydrogen bonds of the C_1 to C_4 alkanes. *J. Photochem.* **1**, 295.

Hanning-Lee, M. A., and M. J. Pilling 1992. Kinetics of the reaction between H atoms and allyl radicals. *Int. J. Chem. Kinet.* **24**, 271–278.

Harding, L. B., R. Guadagnini, and G. C. Schatz 1993. Theoretical studies of the reactions $H + CH \leftrightharpoons C + H_2$ and $H_2 + C \leftrightharpoons CH_2$ using an ab initio global ground-state potential surface for CH_2. *J. Phys. Chem.* **97**, 5472–5481.

Hess, W. P., J. L. Durant, Jr., and F. P. Tully 1989. Kinetic study of the reactions of CN with ethane and propane. *J. Phys. Chem.* **93**, 6402.

Hidaka, Y., T. Nakamura, H. Tanaka, A. Jinno, and H. Kawano 1992. Shock tube and modeling study of propene pyrolysis. *Int. J. Chem. Kinet.* **24**, 761–780.

Hidayat, T., A. Marten, B. Bézard, D. Gautier, T. Owen, H. E. Matthews, and G. Paubert 1997. Millimeter and submillimeter heterodyne observations of Titan: Retrieval of the vertical profile of HCN and the $^{12}C/^{13}C$ ratio. *Icarus* **126**, 170–182.

Homann, K. H., and H. Schweinfurth 1981. Kinetics and mechanism of hydrocarbon formation in the system C_2H_2/O/H. *Ber. Bunsenges. Phys. Chem.* **85**, 569–577.

Homann, K. H., and Ch. Wellmann 1983. Kinetics and mechanism of hydrocarbon formation in the system C_2H_2/O/H at temperatures up to 1300 K. *Ber. Bunsenges. Phys. Chem.* **87**, 609.

Hoobler, R. J., and S. R. Leone 1997. Rate coefficients for reactions of ethynyl radical (C_2H) with HCN and CH_3CN: Implications for the formation of complex nitriles on Titan. *J. Geophys. Res.* **102**, 28717–28723.

Hoobler, R. J., B. J. Opansky, and S. R. Leone 1997. Low-temperature rate coefficients for reactions of ethynyl radical (C_2H) with propane, isobutane, n-butane and neopentane. *J. Phys. Chem.* **101**, 1338–1342.

Hourdin, F., and A. Armengaud 1999. Test of a hierarchy of finite-volume schemes for transport of trace species in an atmospheric general circulation model. *Monthly Weather Rev.* **127**, 822–837.

Hourdin, F., O. Talagrand, R. Sadourny, R. Courtin, D. Gautier, and C. P. McKay 1995. Numerical simulation of the general circulation of the atmosphere of Titan. *Icarus* **117**, 358–374.

Hudson, R. D. 1971. Critical review of ultraviolet photoabsorption cross sections for molecules of astrophysical and aeronomic interest. *Rev. Geophys. Space Phys.* **9**, 305–406.

Hunten, D. M. 1975. Vertical transport in atmospheres. In *Atmospheres of Earth and the Planets* (B. M. McCormac, Ed.), pp. 59–72. Reidel Dordrecht.

Husain, D., and A. X. Ioannou 1997. Reactions of atomic carbon, C[2p2(3PJ)], with dienes and diynes investigated by time-resolved atomic resonance

absorption spectroscopy in the vacuum ultraviolet. *J. Chem. Soc. Faraday Trans.* **93**, 3625–3629.

Husain, D., and L. J. Kirsch 1971. Reactions of atomic carbon by kinetic absorption spectroscopy in the vacuum ultraviolet. *Trans. Faraday Soc.* **67**, 2025.

Husain, D., and A. N. Young 1975. Kinetic investigation of ground-state carbon atoms. *J. Chem. Soc. Faraday Trans. 2* **71**, 525.

Ivin, K. J., and E. W. R. Steacie 1951. The disproportionation and combination of ethyl radicals: the photolysis of mercury diethyl. *Proc. R. Soc. London A* **208**, 25.

Jackson, W. M., D. S. Anex, R. E. Continetti, B. A. Balko, and Y. T. Lee 1991. Molecular beam studies of the photolysis of allene and the secondary photodissociation of the C_3H_x fragments. *J. Chem. Phys.* **95**, 7327–7336.

Kerr, J. A., and M. J. Parsonage 1972. Evoluated Kinetic Data on Gas Phase Addition Reactions. Reactions of Atoms and Radicals with Alkenes, Alkynes and Aromatic Compounds. Butterworths, London.

Kinsman, A. C., and J. M. Roscoe 1994. A kinetic analysis of the photolysis of mixtures of acetone and propylene. *Int. J. Chem. Kinet.* **26**, 191–200.

Kley, D., N. Washida, and W. Groth 1974. Mechanism of CN^* production in flames of active nitrogen with cyaŝnogen. *Ber. Bunsenges. Phys. Chem.* **78**, 205.

Knyazev, V. D., A. Bencsura, S. I. Stoliarov, and I. R. Slagle 1996. Kinetics of the $C_2H_3 + H_2 \leftrightharpoons H + C_2H_4$ and $CH_3 + H_2 \leftrightharpoons H + CH_4$ reactions. *J. Phys. Chem.* **100**, 11346.

Kraus, H., C. Oehlers, F. Temps, H. Gg. Wagner, and M. Wolf 1993. Rate constants for the reactions of $CH_2(X^3B_1)$ with selected alkenes at temperatures between 296 and 728 K. *Ber. Bunsenges. Phys. Chem.* **97**, 545–553.

Lara, L. M., E. Lellouch, J. J. López-Moreno, and R. Rodrigo 1996. Vertical distribution of Titan's atmospheric neutral constituents. *J. Geophys. Res.* **101**, 23,261–23,283.

Lara, L. M., E. Lellouch, and V. Shematovich 1999. Titan's atmospheric haze: the case for HCN incorporation. *Astron. Astrophys.* **341**, 312–317.

Laufer, A. H., E. P. Gardner, T. L. Kwok, and Y. L. Yung 1983. Computations and estimates of rate coefficients for hydrocarbon reactions of interest to the atmospheres of the outer solar system. *Icarus* **56**, 560–567.

Lebonnois, S., and D. Toublanc 1999. Actinic fluxes in Titan's atmosphere, from one to three dimensions: Applications to high-latitude composition. *J. Geophys. Res.* **104**, 22,025–22,034.

Lee, L. C. 1980. $CN(A^2\Pi_i \rightarrow X^2\Sigma^+)$ and $CN(B^2\Sigma^+ \rightarrow X^2\Sigma^+)$ yields from HCN photodissociation. *J. Chem. Phys.* **72**, 6414–6421.

Lellouch, E., A. Coustenis, D. Gautier, F. Raulin, N. Dubouloz, and C. Frère 1989. Titan's atmosphere and hypothesized ocean: A reanalysis of the Voyager 1 radio-occultation and IRIS 7.7 μm data. *Icarus* **79**, 328–349.

Liao, Q., and E. Herbst 1995. Capture calculations for the rates of important neutral-neutral reactions in dense interstellar clouds: $C + C_2H_2$ and $CN + C_2H_2$. *Astrophys. J.* **444**, 694–701.

Lias, S. G., G. J. Collin, R. E. Rebbert, and P. Ausloos 1970. Photolysis of ethane at 11.6–11.8 eV. *J. Chem. Phys.* **52**, 1841–1851.

Lisy, J. M., and W. Klemperer 1980. Electric deflection studies of metastable acetylene. *J. Chem. Phys.* **72**, 3880–3883.

Lungard, R., and J. Heicklen 1984. Pyrolysis of vinylacetylene between 300 and 450°C. *Int. J. Chem. Kinet.* **16**, 125.

Luz, D., and F. Hourdin 1999. Transport of chemical species by transient eddies in the stratosphere of Titan. *Bull. Am. Astron. Soc.* **31**, 1136.

Marston, G., F. L. Nesbitt, and L. J. Stief 1989. Branching ratios in the $N + CH_3$ reaction: formation of the methylene amidogen (H_2CN) radical. *J. Chem. Phys.* **91**, 3483–3491.

Martinotti, F. F., M. J. Welch, and A. P. Wolf 1968. The reactivity of thermal carbon atoms in the gas phase. *Chem. Commun.* **3**, 115.

McKay, C. P. 1996. Elemental composition, solubility and optical properties of Titan's organic haze. *Planet. Space Sci.* **44**, 741–747.

Meaburn, G. M., and S. Gordon 1968. Pulse radiolysis of ammonia gas rate of disappearance of the $NH^3\Sigma$ radical. *J. Phys. Chem.* **72**, 1592.

Monks, P. S., P. N. Romani, F. L. Nesbitt, M. Scanlon, and L. J. Stief 1993. The kinetics of the formation of nitrile compounds in the atmosphere of Titan and Neptune. *J. Geophys. Res.* **98**, 17115–17122.

Monks, P. S., F. L. Nesbitt, W. A. Payne, M. Scanlon, L. J. Stief, and D. E. Shallcross 1995. Absolute rate constant and product branching ratios for the reaction between H and C_2H_3 at $T = 213$ and 298 K. *J. Phys. Chem.* **99**, 17151–17159.

Mordaunt, D. H., I. R. Lambert, G. P. Morley, M. N. R. Ashfold, R. N. Dixon, and C. M. Western 1993. Primary product channels in the photodissociation of methane at 121.6 nm. *J. Chem. Phys.* **98**, 25054–2065.

Mount, G. H., and H. W. Moos 1977. Photoabsorption cross sections of methane and ethane, 1380–1600 Å, at $T = 295$ K and $T = 200$ K. *Astrophys. J.* **214**, L47–L49.

Mount, G. H., E. S. Warden, and H. W. Moos 1977. Photoabsorption cross sections of methane from 1400 to 1850 Å. *Astrophys. J.* **214**, L47–L49.

Natayama, T., and K. Watanabe 1964. Absorption and photoionization coefficients of acetylene, propyne and 1-butyne. *J. Chem. Phys.* **40**, 558–561.

Nava, D. F., M. B. Mitchell, and L. J. Stief 1986. The reaction $H + C_4H_2$: absolute rate constant measurement and implication for atmospheric modeling of Titan. *J. Geophys. Res.* **91**, 4585–4589.

Nesbitt, F. L., G. Marston, and L. J. Stief 1990. Kinetic studies of the reactions of H_2CN and D_2CN radicals with N and H. *J. Phys. Chem.* **94**, 4946–4951.

Niedzielski, J., W. Makulski, and J. Gawlowski 1982. Gas phase photolysis of propylene at 8.4 and 10.0 eV. *J. Photochem.* **19**, 123–131.

Nuth, J. A., and S. Glicker 1982. The vacuum ultraviolet spectra of HCN, C_2N_2, and CH_3CN. *J. Quant. Spectrosc. Radiat. Transfer* **28**, 223–231.

Okabe, H. 1978. *Photochemistry of Small Molecules.* Wiley, New York.

Okabe, H. 1981. Photochemistry of acetylene at 1470 Å. *J. Chem. Phys.* **75**, 2772–2778.

Okabe, H. 1983. Photochemistry of acetylene. *Can. J. Chem* **61**, 850–855.

Okabe, H., and D. A. Becker 1963. Vacuum ultraviolet photochemistry. VII. Photolysis of n-butane. *J. Chem. Phys.* **39**, 2549–2555.

Opansky, B. J., and S. R. Leone 1996a. Low-temperature rate coefficients of C_2H with CH_4 and CD_4 from 154 to 359 K. *J. Phys. Chem.* **100**, 4888–4892.

Opansky, B. J., and S. R. Leone 1996b. Rate coefficients of C_2H with C_2H_4, C_2H_6 and H_2 from 150 to 359 K. *J. Phys. Chem.* **100**, 19904–19910.

Parkes, D. A., D. M. Paul, C. P. Quinn, and R. C. Robson 1973. The ultraviolet absorption by alkylperoxy radicals and their mutual reactions. *Chem. Phys. Lett.* **23**, 425–429.

Pitts, W. M., L. Pasternack, and J. R. McDonald 1982. Temperature dependence of the $C_2(X^1\Sigma_g^+)$ reaction with H_2 and CH_4 and $C_2(X^1\Sigma_g^+$ and $a^3\Pi_u$ equilibrated states) with O_2. *Chem.Phys.* **68**, 417–422.

Pratt, G. L., and S. W. Wood 1984. Kinetics of the reaction of methyl radicals with oxygen. *J. Chem. Soc. Faraday Trans. 1* **80**, 3419–3427.

Rabalais, J. W., J. M. McDonald, V. Scherr, and S. P. McGlynn 1971. Electronic spectroscopy of isoelectronic molecules. *Chem. Rev.* **71**, 94–95.

Rannou, P., M. Cabane, E. Chassefière, R. Botet, C. P. McKay, and R. Courtin 1995. Titan's geometric albedo: Role of the fractal structure of the aerosols. *Icarus* **118**, 355–372.

Rannou, P., C. P. McKay, R. Botet, and M. Cabane 1999. Semi-empirical model of absorption and scattering by isotropic fractal aggregates of spheres. *planet. Space Sci.* **47**, 385–396.

Samson, J. A. R., F. F. Marmo, and K. Watanabe 1962. Absorption and photoionization coefficients of propylene and butene-1 in the vacuum ultraviolet. *J. Chem. Phys.* **36**, 783–786.

Samson, J. A. R., G. N. Haddad, T. Masuoka, P. N. Pareek, and D. A. L. Kilcoyne 1989. Ionization yields total absorption and dissociative photoionization cross sections of CH_4 from 110 to 950 Å. *J. Chem. Phys.* **90**, 6925–6932.

Scherzer, K., P. Claus, and M. Karwath 1985. Untersuchungen sur kinetik und zum mechanismus der addition von methylradicalen an vinylacetylen. *Z. Chem. Phys. (Leipzig)* **266**, 321.

Schwanebeck, W., and J. Warnatz 1975. Reaktionen des butadiins. I. Die reaktion mit wasserstoffatomen. *Ber. Bunsenges. Phys. Chem.* **79**, 530–535.

Sillesen, A., E. Ratajczak, and P. Pagsberg 1993. Kinetics of the reactions H + $C_2H_4 \rightarrow C_2H_5$, H + $C_2H_5 \rightarrow 2\ CH_3$ and $CH_3 + C_2H_5 \rightarrow$ products studied by pulse radiolysis combined with infrared diode laser spectroscopy. *Chem. Phys. Lett.* **201**, 171–177.

Sims, I. R., J.-L. Queffelec, D. Travers, B. Rowe, L. B. Herbert, J. Karthäuser, and I. W. M. Smith 1993. Rate constants for the reactions of CN with hydrocarbons at low and ultra-low temperatures. *Chem. Phys. Lett.* **211**, 461–468.

Slack, M. W. 1976. Kinetics and thermodynamics of the CN molecule. III. Shock tube measurement of CN dissociation rates. *J. Chem. Phys.* **64**, 228.

Smith, G. R., D. F. Strobel, A. L. Broadfoot, B. R. Sandel, D. E. Shemansky, and J. B. Holberg 1982. Titan's upper atmosphere: Composition and temperature from the EUV solar occultation results. *J. Geophys. Res.* **87**, 1351–1359.

Smith, N. S. 1999. Sensibilité des modèles théoriques de l'atmosphère de Titan aux incertitudes sur la photochimie des hydrocarbures simples. Ph.D. thesis, Université Paris XII Val de Marne.

Smith, N. S., and F. Raulin 1999. Modeling of methane photolysis in the reducing atmospheres of the outer solar system. *J. Geophys. Res.* **104**, 1873–1876.

Smith, P. L., K. Yoshino, and W. H. Parkinson 1991. High-resolution, VUV (147–201 nm) photoabsorption cross sections for C_2H_2 at 195 and 195 K. *J. Geophys. Res.* **96**, 17529–17533.

Smith, N. S., Y. Bénilan, and P. Bruston 1998. The temperature dependent absorption cross sections of C_4H_2 at mid-ultraviolet wavelengths. *Planet Space Sci.* **46**, 1215–1220.

Stewart, P. H., C. W. Larson, and D. M. Golden 1989. Pressure and temperature dependence of reactions proceeding via a bound complex. II. Application to $2\ CH_3 \rightleftharpoons C_2H_5$ + H. *Combust. Flame* **75**, 25.

Strobel, D. F. 1982. Chemistry and evolution of Titan's atmosphere. *Planet. Space Sci.* **30**, 839–848.

Strobel, D. F., M. E. Summers, and X. Zhu 1992. Titan's upper atmosphere: Structure and ultraviolet emissions. *Icarus* **100**, 512–526.

Sun, Q., D. L. Yang, N. S. Wang, J. M. Bowman, and M. C. Lin 1990. Experimental and reduced dimensionality quantum rate coefficients for H_2 (D_2) + CN $\leftrightharpoons$ H(D)CN + H(D). *J. Chem. Phys.* **93**, 4730.

Tanguy, L., B. Bézard, A. Marten, D. Gautier, E. Gérard, G. Paubert, and A. Lecacheux 1990. Stratospheric profil of HCN on Titan from millimeter observations. *Icarus* **85**, 43–57.

Teng, L., and W. E. Jones 1972. Kinetics of the reactions of hydrogen atoms with ethylene and vinyl fluoride. *J. Chem. Soc. Faraday Trans. 1* **68**, 1267–1277.

Tokano, T., F. M. Neubauer, M. Laube, and C. P. McKay 1999. Seasonal variation of Titan's atmospheric structure simulated by a general circulation model. *Planet. Space Sci.* **47**, 493–520.

Toublanc, D., J. P. Parisot, J. Brillet, D. Gautier, F. Raulin, and C. P. McKay 1995. Photochemical modeling of Titan's atmosphere. *Icarus* **113**, 2–26.

Tsang, W. 1988. Chemical kinetic data base for combustion chemistry. III. Propane. *J. Phys. Chem. Ref. Data* **17**, 887–951.

Tsang, W. 1991. Chemical kinetic data base for combustion chemistry. V. Propene. *J. Phys. Chem. Ref. Data* **20**, 221–274.

Tsang, W., and R. F. Hampson 1986. Chemical kinetic data base for combustion chemistry. I. Methane and related compounds. *J. Phys. Chem. Ref. Data* **15**, 1087–1279.

Van Leer, B. 1977. Towards the ultimate conservative difference scheme: IV. A new approach to numerical convection. *J. Comput. Phys.* **23**, 276–299.

Vervack, R. J., Jr., B. R. Sandel, and D. F. Strobel 1999. First results from a reanalysis of the Voyager I ultraviolet spectrometer solar occultations by Titan. *Icarus*, submitted.

Wagner, H., Gg., and R. Zellner 1972a. Reaktionen von wasserstoffatomen mit ungesättigten C_3-kohlenwasserstoffen. II. Die reaktion von H atomen mit methylacetylen. *Ber. Bunsenges. Phys. Chem.* **76**, 518–525.

Wagner, H. Gg., and R. Zellner 1972b. Reaktionen von wasserstoffatomen mit ungesättigten C_3-kohlenwasserstoffen. III. Die reaktion von H atomen mit allen. *Ber. Busenges. Phys. Chem.* **76**, 667–672.

Westmoreland, P. R., A. M. Dean, J. B. Howard, and J. P. Longwell 1989. Forming benzene in flames by chemically activated isomerization. *J. Phys. Chem.* **93**, 8171.

Whyte, A. R., and L. F. Phillips 1983. Rate of reaction of N with CN(v = 0, 1). *Chem. Phys. Lett.* **98**, 590–593.

Wilson, E. H., and S. K. Atreya 1999. Sensitivity studies of methane photolysis and its impact on hydrocarbon chemistry in the atmosphere of Titan. *Bull. Am. Astron. Soc.* **31**, 1142.

Yang, D. L., T. Yu, M. C. Lin, and C. F. Melius 1992a. CN radical reactions with hydrogen cyanide and cyanogen: comparison of theory and experiment. *J. Chem. Phys.* **97**, 222–226.

Yang, D. L., T. Yu, N. S. Wang, and M. C. Lin 1992b. CN radical reactions with selected olefins in the temperature range 174–740 K. *Chem. Phys.* **160**, 317–325.

Yang D. L., T. Yu, M. C. Lin, and C.F.Melius 1993. The reaction of CN with CH_4 and CD_4: An experimental and theoetical study. *Chem. Phys.* **177**, 271–280.

Yelle, R. V. 1991. Non-LTE models of Titan's upper atmosphere. *Astrophys. J.* **383**, 380–400.

Yung, Y. L. 1987. An update of nitrile photochemistry on Titan. *Icarus* **72**, 468–472.

Yung, Y. L., M. Allen, and Pinto J. P. 1984. Photochemistry of the atmosphere of Titan: Comparison between model and observations. *Astrophys. J. Supp.* **55**, 465–506.

Zabarnick, S., and M. C. Lin 1989. Kinetics of CN($X^2\Sigma^+$) radical reactions with HCN, BrCN and CH_3CN. *Chem. Phys.* **134**, 185–191.

Zelikoff, M., and K. Watanabe 1953. Absorption coefficients of ethylene in the vacuum ultraviolet. *J. Opt. Soc. Am.* **43**, 756–759.

Zwier, T. S., and M. Allen 1996. Metastable diacetylene reactions as routes to large hydrocarbons in Titan's atmosphere. *Icarus* **123**, 578–583.